Neuron
Article

The Projective Field of Retinal Bipolar Cells and Its Modulation by Visual Context

Hiroki Asari[1,2] and Markus Meister[1,2,*]
[1]Department of Molecular and Cellular Biology and Center for Brain Science, Harvard University, Cambridge, MA 02138, USA
[2]Present address: Division of Biology and Biological Engineering, California Institute of Technology, Pasadena, CA 91125, USA
*Correspondence: meister@caltech.edu
http://dx.doi.org/10.1016/j.neuron.2013.11.029

SUMMARY

The receptive field of a sensory neuron spells out all the receptor inputs it receives. To understand a neuron's role in the circuit, one also needs to know its projective field, namely the outputs it sends to all downstream cells. Here we present the projective fields of the primary excitatory neurons in a sensory circuit. We stimulated single bipolar cells of the salamander retina and recorded simultaneously from a population of ganglion cells. Individual bipolar cell signals diverge through polysynaptic pathways into ganglion cells of many different types and over surprisingly large distance. However, the strength and polarity of the projection depend on the cell types involved. Furthermore, visual stimulation strongly modulates the bipolar cell projective field, in opposite direction for different cell types. In this way, the context from distant parts of the visual field can control the routing of signals in the inner retina.

INTRODUCTION

The retina has two synaptic layers to encode visual stimuli into a series of spike trains (Masland, 2012). First, in the outer retina, photoreceptors convert light into electrical signals and send them to bipolar cells. Horizontal cells apply a level of gain control and lateral inhibition at this synaptic layer (Wu, 1994). Second, in the inner retina, bipolar cells transmit the signals to ganglion cells, modified by intricate interactions with amacrine cells (Baccus, 2007). The ganglion cell population comprises many distinct types and each type's visual response properties are thought to derive from a specific combination of bipolar and amacrine cell signals (Vaney et al., 2012). The diversity of these interactions in the inner retina is one of the least understood aspects of retinal processing.

As in other sensory systems, a central tool in studying circuitry of the retina has been the measurement of receptive fields. A neuron's receptive field spells out how its visual responses arise from the convergence of receptor signals. By comparing receptive fields of neurons along the processing chain, one gains insight into how the circuit is structured (Gollisch and Meister, 2010; Roska and Werblin, 2001). For a more complete assessment of circuit function, it would be useful also to know the neuron's "projective field," namely how its signals diverge to all downstream partners (Lehky and Sejnowski, 1988). Recent advances in experimental methods made it possible to measure the impact of a single retinal neuron on many of its projection targets (Asari and Meister, 2012; Baccus et al., 2008; Field et al., 2010), which enables a complete projective field analysis (de Vries et al., 2011; Doi et al., 2012). Here we measure the projective fields of the principal excitatory neurons in a sensory pathway.

By simultaneously recording from multiple ganglion cells while controlling the activity of individual bipolar cells intracellularly, we explored how bipolar cells distribute their signals to the subsequent ganglion cell population in the salamander retina. This signal flow is subject to some clear anatomical constraints: many bipolar cell types have axon terminals only at specific laminae of the inner plexiform layer (Pang et al., 2004; Wässle et al., 2009; Wu et al., 2000), and similarly many ganglion cell types show lamina-specific dendritic arborizations (Masland, 2012; Siegert et al., 2009; Toris et al., 1995; Völgyi et al., 2009). Therefore, direct synaptic connections should be limited to only certain pairings of cell types. However, the full projective field includes polysynaptic connections as well. We will show that this leads to considerably broader spread of bipolar cell signals than expected from laminar connectivity alone, both regarding the cell types involved and the spatial extent of signal flow. Furthermore, the projective field of a given bipolar cell can be modulated profoundly by distant visual stimuli that are outside its receptive field.

RESULTS

Bipolar cells occupy a special place in retinal circuitry: they are the only link from the outer retina to the inner retina. How does the signal of a given bipolar cell diverge into the population of ganglion cells at the output of the retina? To address this question, we manipulated the membrane potential of an individual bipolar cell intracellularly and simultaneously recorded the spiking activity of many nearby ganglion cells in the isolated salamander retina. The goal was to observe the influence of one bipolar cell on all the retina's output neurons, involving not only direct synaptic connections but the entire circuit of the inner retina. Following prior usage, we term this the "projective field," and we will refer to the influence of a bipolar cell on a specific ganglion cell—which may be polysynaptic—as its "projection" to that neuron. Because the intracellular recordings in the inner nuclear layer were performed blind, we also encountered a good number of

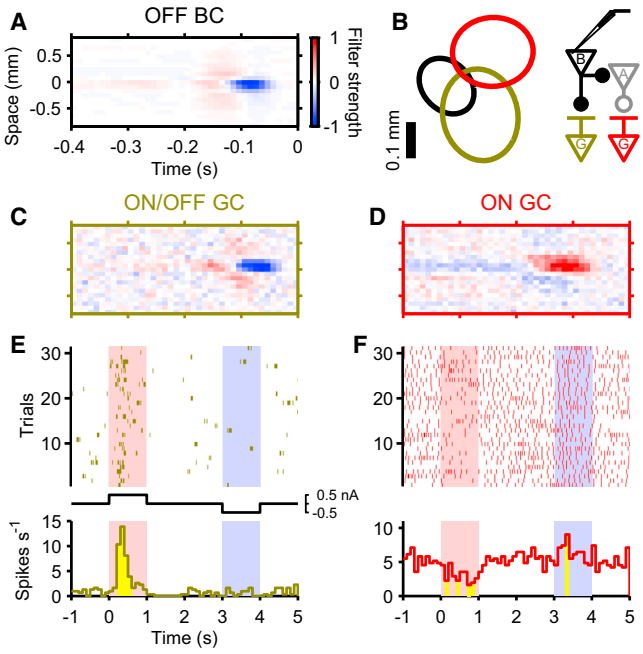

Figure 1. Ganglion Cells Show Distinct Responses to Inputs from a Single Bipolar Cell

(A–D) The spatiotemporal receptive field of a bipolar cell (A) and of two ganglion cells (C and D). For simplicity, all the spatiotemporal receptive fields are shown only for one spatial dimension at the receptive field center (red hue, On-polarity; blue hue, Off-polarity). The full spatial profiles and the relative position of the cells are indicated by the outlines in (B) (contour at 1 SD from a two-dimensional Gaussian fit; black, bipolar cell in A; olive, ganglion cell in C; red, ganglion cell in D).

(E and F) Raster graph (top) and peristimulus time histogram (bottom) of the spikes from the two representative ganglion cells (E and F; from C and D, respectively) simultaneously recorded in response to current injection into the single bipolar cell (from A; pink, depolarization; blue, hyperpolarization). The yellow-shaded bins indicate significant changes in the ganglion cell firing rate from its baseline activity. The schematic circuit diagram in (B) shows a parsimonious interpretation of the observation (A, amacrine cell; B, bipolar cell; G, ganglion cell; closed circle, excitatory synapse; open circle, inhibitory synapse).

amacrine cells and subjected them to the same analysis. These results will serve as useful reference points for some of the following sections.

Depolarization or hyperpolarization of a bipolar cell frequently produced changes in spiking of ganglion cells (Figure 1). In most cases, ganglion cell spikes were evoked when a bipolar cell was depolarized from the resting potential (Figure 1E) or returned from hyperpolarization to the resting potential, indicating a sign-preserving projection between the two neurons. Less frequently, we observed sign-inverting projections, where the ganglion cell fired on hyperpolarization of the bipolar cell (Figure 1F). These must be mediated by inhibitory amacrine cells, because direct synaptic transmission from bipolar cells is excitatory (Masland, 2012), even though some bipolar cells express the transmitter γ-aminobutyric acid (GABA) along with glutamate (Yang and Wang, 1999). It is reassuring that these methods of pairwise recording of bipolar and ganglion cells reveal not only direct synaptic connections but also indirect effects that pass through amacrine cell circuits.

In this study, we begin by analyzing the general properties of the bipolar cell projective field, such as its spatial profile and dynamics. With pharmacological tools, we assess the contribution of intervening circuitry to the spatial extent of the projective field, including amacrine cell inhibitory networks and gap junction electrical networks. In the second part, we classify the bipolar and ganglion cells into distinct response types and determine more specifically how the projections are constrained by the identities of source and target neuron. Finally, we investigate how the bipolar cell projective field changes depending on the context from visual stimulation.

Bipolar Cells Have Large Projective Fields

To map the bipolar cell projective field, we first measured the distance and the projection strength for each recorded pair of bipolar and ganglion cells. Specifically, the distance between the cells was taken as the separation between their receptive field centers (obtained from white-noise analysis; e.g., Figures 1A–1D). The projection strength was calculated as the difference of the ganglion cell firing rates in response to bipolar cell depolarization and hyperpolarization, normalized by the pooled SD across trials (Equation 2; e.g., Figures 1E and 1F). In each case, we evaluated whether the projection was statistically different from zero.

The resulting projective field of bipolar cells showed several prominent features (Figures 2 and 3). First, the projection strength could have different signs and values even at the same distance. Thus, the same bipolar cell sent both sign-preserving and sign-inverting signals to different ganglion cells (Figure 2A). In general, however, sign-preserving projections from bipolar cells dominated in our data set (Figure 3A–3D), regardless of the baseline ganglion cell firing properties (Figure S1 available online). By contrast, amacrine cells primarily showed sign-inverting projections to ganglion cells (Figures 2B and 3E–3H), as expected from their roles as inhibitory interneurons. Thus, the paucity of sign-inverting projections from bipolar cells is not due to any difficulty in detecting ganglion cell inhibition; instead, it seems that monosynaptic connections are simply easier to detect than disynaptic projections that require the excitation of an intervening interneuron.

Second, the bipolar projective field is sparse, meaning that at any given distance only a fraction of ganglion cells receive a significant projection. For sign-preserving projections, the probability was ~50% for an immediately adjacent ganglion cell and decayed strongly with increasing distance (Figure 3B). For sign-inverting projections, the probability was more than 10-fold lower (Figure 3B). By contrast, amacrine cells had frequent sign-inverting projections to ganglion cells, again with a strong distance dependence (Figure 3F).

Third, the projections involved significant dynamics. After the onset of a current pulse into the bipolar cell, the ganglion cell firing rate generally rose to a peak and then declined again (Figure 1E). We summarized the time dependence by measuring the latency of the peak. This peak latency varied dramatically across different projections, from ~10 ms to ~1 s (Figures 3C and 3D). One might expect that a weaker projection would have a longer

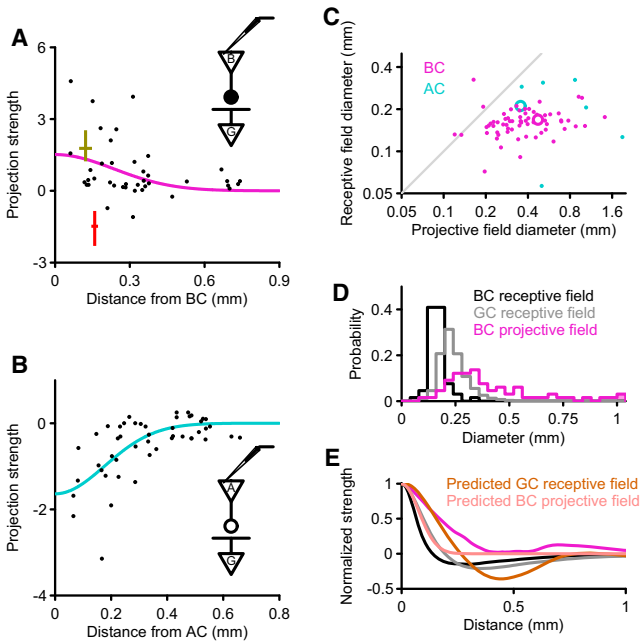

Figure 2. The Projective Field Is Larger Than the Receptive Field

(A) Projective field of a single bipolar cell (from Figure 1; violet, Gaussian curve fit from Equation S3). Each data point represents projection onto one ganglion cell (Equation S2; olive and red points from Figures 1C and 1D, respectively; 95% confidence intervals are shown for these representative data).

(B) Projective field of an amacrine cell displayed as in (A) (cyan, Gaussian curve fit).

(C) The projective fields of bipolar cells (violet; 0.42 ± 0.24 mm; mean diameter ± SD; n = 66 cells) and amacrine cells (cyan; 0.79 ± 0.55 mm; n = 7 cells) are generally larger than their own receptive fields (0.16 ± 0.04 mm for bipolar cells, $p < 0.001$; 0.22 ± 0.10 mm for amacrine cells, $p = 0.016$). Circles indicate the examples in (A) and (B), respectively. Note logarithmic axes.

(D) The bipolar cell projective field (violet) is not only larger than its receptive field (black) but can even exceed many ganglion cell receptive fields (gray; 0.24 ± 0.07 mm, $p < 0.001$; n = 4,236 cells). The filled bar on the rightmost bin indicates fields larger than 1 mm.

(E) The spatial profile of projective and receptive fields (color coded as in D for the measured ganglion cell receptive field and the measured bipolar cell receptive and projective fields; brown and pink, predicted ganglion cell receptive field and bipolar cell projective field, respectively, as derived from Equation 1).

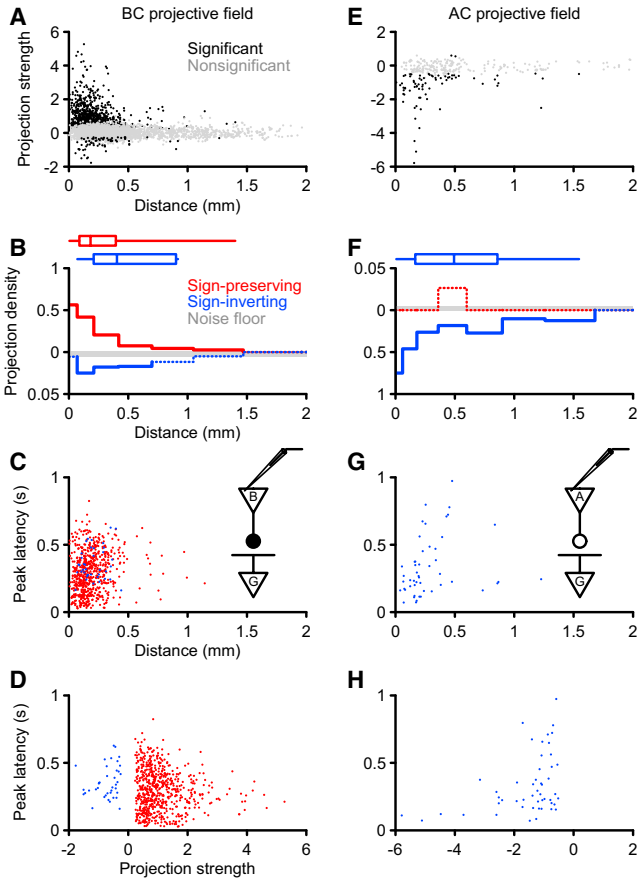

Figure 3. Polarity, Strength, and Range of the Projective Field

(A) Population data of the projection strength as a function of the distance between bipolar and ganglion cells (black, significant; gray, nonsignificant).

(B) Density of bipolar cell projections as a function of distance (solid, significant; dotted, nonsignificant; this convention applies to all subsequent plots of this kind). Density is measured as the fraction of ganglion cells with a significant projection, either sign-preserving (red) or sign-inverting (blue; shown upside-down for display purpose, note different axis scale). Box plot (top) represents the minimum, first quartile, median, third quartile, and maximum values above the noise floor (gray).

(C) Peak latency of ganglion cell firing rates evoked by bipolar cell current injection (from Equation S4), plotted against the distance between the cells (correlation coefficient $R = 0.15$ with $p < 0.001$ for sign-preserving projection, red; $R = 0.15$ with $p > 0.35$ for sign-inverting projection, blue).

(D) Peak latency of ganglion cell firing rates, plotted against the projection strength ($R = -0.09$ with $p = 0.02$ for sign-preserving projection, red; $R = 0.23$ with $p > 0.14$ for sign-inverting projection, blue).

(E–H) Population data for the amacrine cell projective field, displayed as in (A)–(D). No significant sign-preserving projections were observed.

latency, because it may take longer to depolarize the target neuron, but this was not the case: even at the same projection strength one found all possible latencies (Figure 3D). There was a small increase of latency with projection distance (Figure 3C), but again this correlation accounted for only a fraction of the range. We conclude that bipolar cells drive ganglion cells with a wide variety of dynamics (Asari and Meister, 2012).

Finally, the bipolar cell projections covered a surprisingly large distance. Averaging over the wide variation in projection strength even to adjacent ganglion cells, one can approximate the projection with a Gaussian profile (Figure 2A; Equation S3). These profiles ranged in diameter from 100 μm to more than 1 mm, with an average of 0.42 mm (Figures 2C and 2D). This was considerably larger than the bipolar cell receptive field diameter of 0.16 mm. It appears therefore that lateral signal flow extends considerably farther in the inner retina (from bipolar cells) than in the outer retina (to bipolar cells). In the following section, we will consider the circuits underlying this lateral distribution.

Polysynaptic Transmission of Bipolar Cell Signals via Amacrine Cells and Gap Junctions

How can a bipolar cell excite ganglion cells more than 1 mm away (Figure 3)? This distance exceeds what one expects for monosynaptic transmission, because the combined radius of

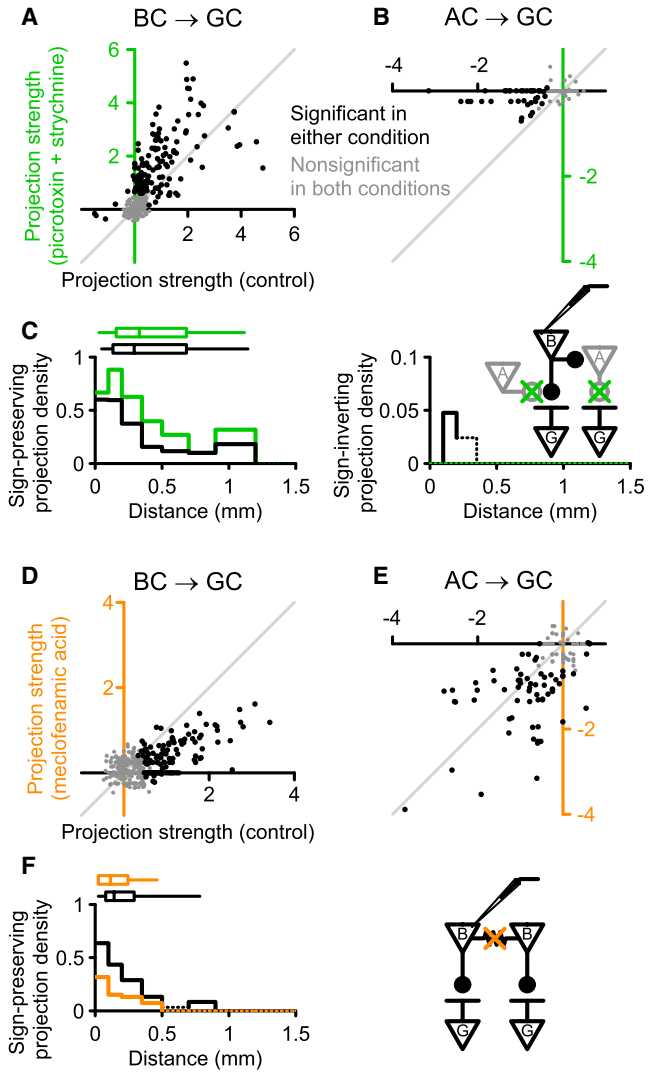

Figure 4. Inner Retinal Circuits Modify Bipolar Cell Projections

(A and B) Projection strength of bipolar cells (A; n = 10 bipolar cells and 283 ganglion cells) and amacrine cells (B; n = 3 amacrine cells and 87 ganglion cells) before and after applying 100 μM picrotoxin and 1.0 μM strychnine (black, significant projection in at least one condition; gray, nonsignificant in both conditions). Blocking inhibitory synaptic transmission enhanced the signals from bipolar cells (A; $p < 0.001$) but suppressed those from amacrine cells (B; $p < 0.001$).

(C) Density of sign-preserving (left) or -inverting (right) projections from bipolar cells to ganglion cells before (black) and after (green) the drug application (displayed as in Figure 3B).

(D and E) Projection strength of bipolar cells (D; n = 8 bipolar cells and 444 ganglion cells) and amacrine cells (E; n = 2 amacrine cells and 143 ganglion cells) before and after applying 100 μM meclofenamic acid (displayed as in A and B). The gap junction blocker suppressed the effects of bipolar cell signals ($p < 0.001$; D) but slightly enhanced those of amacrine cells ($p = 0.04$; E).

(F) Density of bipolar cell projections to ganglion cells before (black) and after (orange) loss of electrical couplings (displayed as in C). Note the contribution of gap junctions to the long-range projections ($p = 0.03$ for those with >0.35 mm). No significant sign-inverting projections were found in this data set.

bipolar cell axonic field and ganglion cell dendritic field is about 0.35 mm (Pang et al., 2004; Wu et al., 2000; Zhang and Wu, 2009, 2010). Polysynaptic pathways must be involved, such as those through electrical synapses (Cook and Becker, 1995; Wong-Riley, 1974) or disinhibitory effects via serial connections of amacrine cells (Eggers and Lukasiewicz, 2010; Manookin et al., 2008). Here we took a pharmacological approach to examine how inner retinal circuits contribute to the bipolar cell projective field (Figures 4 and S2).

We first blocked GABA and glycine transmission by applying 100 μM picrotoxin and 1.0 μM strychnine. This generally leads to an increase in the size of the ganglion cell receptive field (Cook and McReynolds, 1998) but does not substantially affect the bipolar cell receptive field in the salamander retina (Hare and Owen, 1990, 1996). Thus, these inhibitory transmission blockers work mainly on the inner retina (amacrine cells) but not on the outer retina (horizontal cells). Indeed, we found that they greatly suppressed the projection strength between amacrine cells and ganglion cells (Figure 4B). In contrast, we found a strong increase in the projection strength between bipolar cells and ganglion cells (Figures 4A and S2A–S2C). Many ganglion cells revealed responses to bipolar cell depolarization only after the loss of inhibition (Figure 4C), and no ganglion cells responded to bipolar cell hyperpolarization after the drug application. Little change was found, however, in the spatial extent of the sign-preserving signals from bipolar cells: even with inhibitory circuits blocked, the influence of bipolar cells extended over 1 mm (Figure 4C). On average, it appears that amacrine cells contribute to the projection strength but not to the spatial extent of the bipolar cell projective field. Specifically, we conclude that disinhibition via serial connections of amacrine cells (Eggers and Lukasiewicz, 2010; Manookin et al., 2008) does not account for long-range sign-preserving projections (Figure 3).

We next applied 100 μM meclofenamic acid to block gap junctions (Zhang and Wu, 2009). This drug produced a significant decrease of the bipolar cell projection strength (Figures 4D and S2D–S2F) and a loss of the most distant projections (Figure 4F). In contrast, the drug application had, on average, little effect on the projection strength of amacrine cells (Figure 4E). Although a change in projection strength cannot be distinguished strictly from a change in range, these results suggest that the signals from bipolar cells are distributed not only vertically by direct excitation of ganglion cells but also laterally through gap junction networks (Cook and Becker, 1995; Wong-Riley, 1974). In principle, this could occur through electrical coupling among bipolar cells (Arai et al., 2010) or among ganglion cells or amacrine cells (Vaney, 1991). As elaborated below, OFF bipolar cells systematically had broader projections than ON bipolar cells, regardless of the target ganglion cell type (Figure 6A). Combined with evidence that OFF bipolar cells are more strongly coupled (Zhang and Wu, 2009), this favors an interpretation that invokes lateral signal spread among bipolar cells.

All-to-All Projections between Bipolar and Ganglion Cell Types

The vertebrate retina contains 10–20 types of bipolar cells (McGuire et al., 1984; Pang et al., 2004; Wässle et al., 2009;

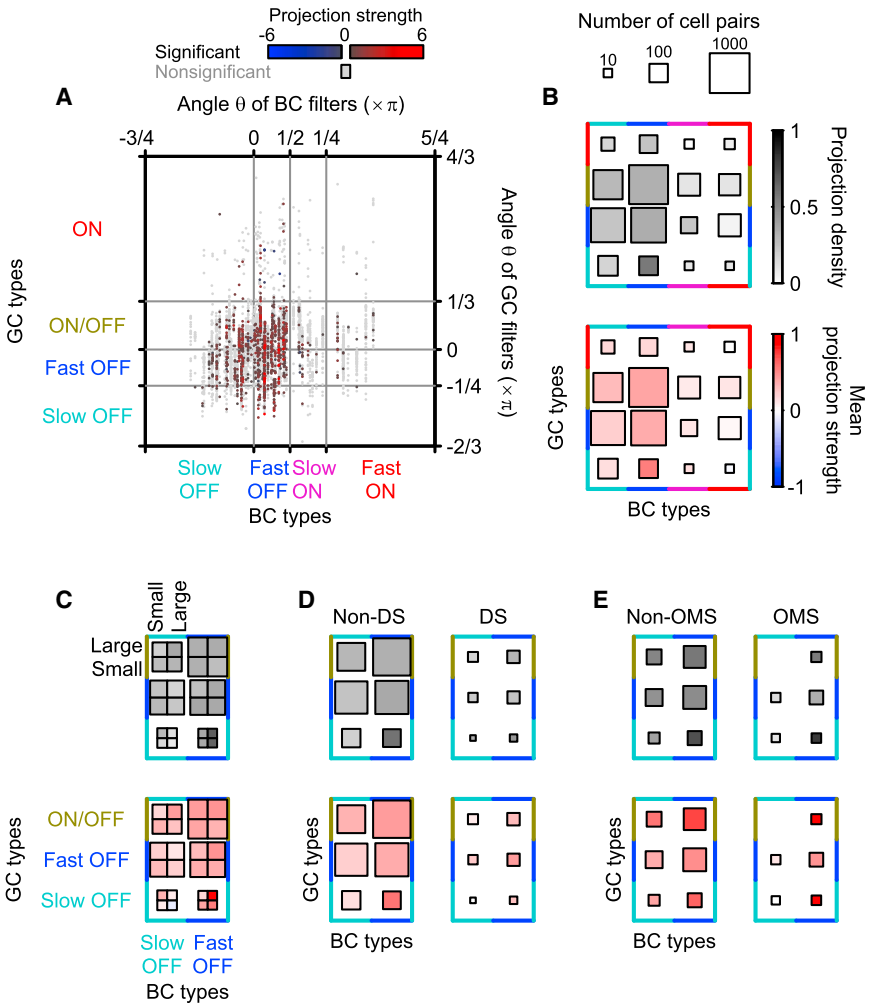

Figure 5. Nearly All-to-All Projections among Different Types of Bipolar and Ganglion Cells

(A) Each data point represents a pair of bipolar and ganglion cells (dark red, significant sign-preserving projection; dark blue, significant sign-inverting projection; gray, nonsignificant projection; from Figure 3A) in the feature space that characterizes the polarity and kinetics of their visual responses (color coded for different cell types; boundaries in dark gray). Horizontal axis is the angular parameter θ that characterizes the bipolar cell temporal filter, and vertical axis is the same for ganglion cells. See Supplemental Experimental Procedures and Figure S3 for details.

(B) Projection patterns across physiologically distinct types of bipolar cells and ganglion cells (top, projection density; bottom, mean projection strength). Square size indicates the number of recorded cell pairs. Cell types are color coded as in (A).

(C) Projection patterns (displayed as in B) from slow OFF and fast OFF bipolar cells to slow OFF, fast OFF, and ON/OFF ganglion cells, each subdivided into two categories based on their receptive field sizes (large and small; Figures S3D and S3H).

(D and E) Bipolar cell projection patterns among the types shown in (C), with ganglion cells further divided into direction-selective (DS) and nonselective cells (from Equation S1; D) or into object motion-sensitive (OMS) and nonsensitive cells (from Equation S2; E).

Wu et al., 2000), whose axonal arbors stratify at different levels of the inner plexiform layer. Because the dendrites of many ganglion cells are similarly stratified (Roska and Werblin, 2001; Masland, 2012), one expects that different bipolar cell types have different projective fields and that those projective fields should be selective for specific ganglion cell types. In the present experiments, the need for simultaneous recording prohibited a morphological analysis of each target cell. Instead, we classified the neurons based on their physiological properties, namely the characteristics of their visual responses. We then analyzed how the projective field depends on the identities of the source bipolar and target ganglion cell. Specifically, we examined the following properties at the population level: the projection density, namely the probability of observing a projection between two types; the strength of the projection; and its spatial extent (Figures 5, 6, S3, and S4).

We first sorted both bipolar and ganglion cells into four subgroups each, based on the polarity and kinetics of their visual responses (Figure S3). At the most basic level, we found significant projections for almost every combination of bipolar and ganglion cell type (Figures 5A and 5B). Some functional types appeared more frequently in these recordings than others; in particular, the ON cell types are comparatively rare for both bipolar and ganglion cells in the salamander retina (Segev et al., 2006; Vallerga and Usai, 1986). Nonetheless, we observed significant projections for all pairings of cell types except from slow ON bipolar cells to ON ganglion cells.

To examine finer projection patterns between bipolar cells and ganglion cells, we subdivided each of the cell types (Figure S3) based on the receptive field sizes, direction selectivity (Vaney et al., 2012), or object motion sensitivity (Ölveczky et al., 2003; Baccus et al., 2008). Here we omitted ON cell types from the analysis due to scarcity of data. All-to-all projection patterns were found even after such finer cell-type classification (Figures 5C–5E). These observations reinforce prior findings of substantial crosstalk among bipolar cell signals (McGuire et al., 1986; Pang et al., 2007; Werblin, 2010), at least in the amphibian retina.

Cell-type-Specific Projective Fields

On the background of this all-to-all connectivity, one can observe clear cell-type-specific features in the projective field. First, OFF bipolar cell types generally had denser and more far-reaching projections than ON types (Figure 6A). Long-distance projections were almost exclusively from OFF bipolar cells (Figure 6A). Furthermore, not only the density but also the strength of projections was greater for OFF than for ON bipolar cell types (Figure S4A). Among the bipolar types we defined,

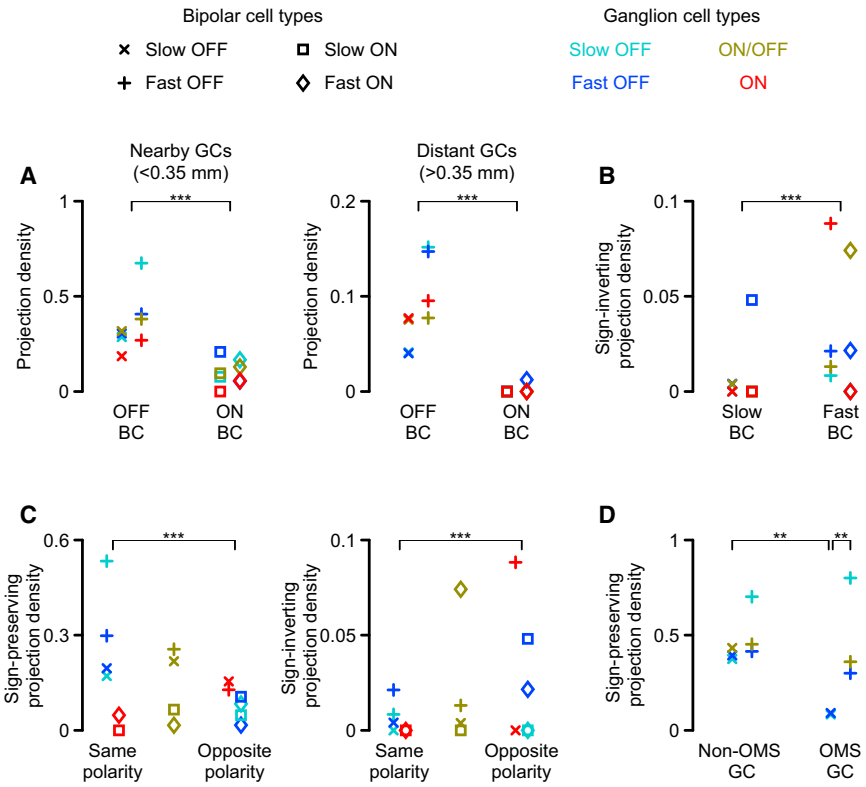

Figure 6. Cell-type-Specific Features of the Bipolar Cell Projective Field

(A) OFF bipolar cells had a higher projection density than ON bipolar cells ("★★★" for $p < 0.001$). Each data point represents projection from a specific bipolar cell type (distinct symbol) to a specific ganglion cell type (color coded). Boundary between nearby (left) and distant (right) cell pairs was set to be the anatomically expected range of monosynaptic transmission.

(B) Bipolar cells with fast response kinetics had a higher probability of making sign-inverting projection than slow bipolar cells.

(C) Sign-preserving projections were denser between cells of the same visual response polarity (left), whereas sign-inverting projections were denser between cells of opposite visual response polarity (right). Projections to ON/OFF ganglion cells were excluded from both comparisons (middle in each panel).

(D) Sign-preserving projections to OMS ganglion cells were denser from fast OFF bipolar cells than from slow OFF cells ("★★" for $p < 0.01$). Projections from slow OFF bipolar cells were denser to non-OMS ganglion cells than to OMS cells.

fast OFF cells had by far the densest and strongest projective fields. At the other end of the range, fast ON cells had the weakest projections.

Second, focusing on the sign-inverting projections, these were observed much more frequently for fast bipolar cell types than for slow types (Figure 6B). This arrangement has a possible significance for circuit function: the responses of ganglion cells often rely intimately on the temporal coincidence of excitatory and inhibitory signals (Münch et al., 2009). Yet the inhibitory signals must pass through one additional interneuron, which entails a time delay. That time delay could be compensated if the bipolar cells driving the inhibitory pathway have shorter response latency. The present results show that this is indeed a systematic feature of bipolar cell projections.

Third, the balance of sign-preserving and sign-inverting projections depended strongly on the response polarity of the bipolar and ganglion cells involved. Although the average strength of bipolar projections was generally sign-preserving (Figure 5), on a case-by-case basis we found both sign-preserving and sign-inverting projections. When bipolar and ganglion cell had the same visual response polarity, sign-preserving connections were more frequent; when they had opposite polarity, sign-inverting projections were more frequent (Figure 6C). Thus, bipolar cells exert both an excitatory "push" and an inhibitory "pull" on different types of ganglion cells, depending on their response polarity. This process, also termed "crossover inhibition" (Werblin, 2010), had previously been observed only from the ganglion cell side. The present observations show that the same bipolar cell type can participate in both push and pull.

Finally, the object motion-sensitive (OMS) ganglion cells in the population received a more restricted set of bipolar projections than non-OMS cells (Figures 6D and S3J). Specifically, the OMS ganglion cells draw their inputs mainly from fast OFF bipolar cells. Note that this arrangement confirms a prediction derived previously from a computational model of the OMS response (Baccus et al., 2008).

Modulation of the Projective Field by Visual Context

The receptive fields of visual neurons are not static response parameters but vary depending on visual context. For example, the receptive field profile of a bipolar cell changes substantially depending on the adapting light level (Werblin, 1970). Similarly, it is important to test whether the projective field of the bipolar cell changes in the context of visual stimulation, as compared to the dark state. One can envision several mechanisms for this. First, consider the recipient ganglion cell. Under a global dynamic visual stimulus, the ganglion cell will receive excitation and inhibition from many interneurons. This will increase the synaptic conductance in the dendritic tree and thus reduce the influence of each additional synaptic input. Thus, one expects a general reduction in the projection strength from any given bipolar cell when the ganglion cells are driven by a visual stimulus. Second, the synaptic transmission from bipolar to ganglion cells is under control of inhibitory synapses from amacrine cells at the bipolar terminal (Dong and Werblin, 1998; Nirenberg and Meister, 1997; Tachibana and Kaneko, 1988). If those amacrine cells are visually driven, one expects a modulation of the projection strength. We performed two kinds of experiments to test for such effects.

First, we exposed the retina to uniform illumination over the whole field, flickering randomly in time. This stimulated firing in

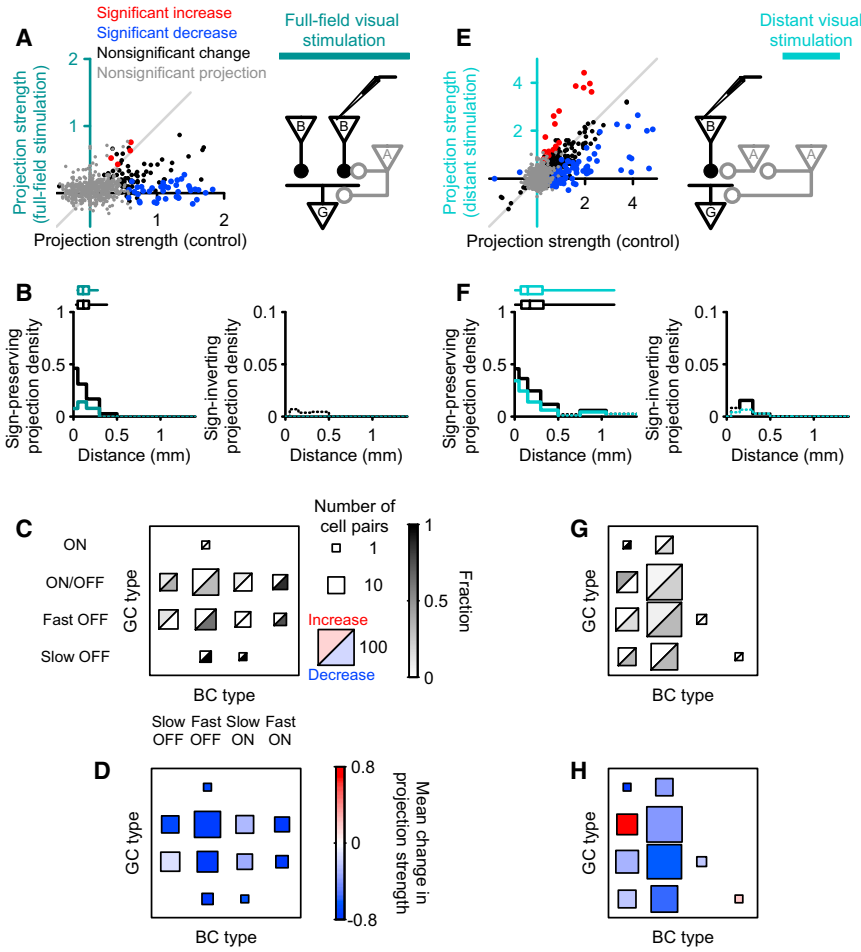

Figure 7. Context-Dependent Modulation of Bipolar Cell Projective Field by Visual Stimulation

(A) Projection strength from bipolar to ganglion cells in the presence and absence of full-field visual stimulation (n = 15 bipolar cells and 731 ganglion cells; gray, nonsignificant projection in both conditions; black, red, and blue, significant projection in at least one condition; red, significant increase during visual stimulation; blue, significant decrease).

(B) Density of sign-preserving (left) or -inverting (right) projection from bipolar cells to ganglion cells with (cyan) or without (black) the full-field visual stimulation (displayed as in Figure 3B).

(C) Effects of visual stimulation on the projection strength among different pairs of bipolar and ganglion cell types (displayed as in Figure 5B). The square size represents the number of cell pairs with significant projection in at least one condition. Grayscale indicates the fraction of cell pairs whose projection strength significantly increased (top left) or decreased (bottom right). Projections from fast bipolar cell types were affected more frequently than from slow types ($p < 0.001$).

(D) Mean change in the projection strength among distinct pairs of bipolar and ganglion cell types (red hue, positive; blue hue, negative; displayed as in Figure 5B). The visual stimulation suppressed projections from fast bipolar cell types more strongly than from slow types ($p < 0.001$).

(E–H) Cell-type-specific modulation of the bipolar cell projective field by visual stimulation in a distant annulus (n = 27 bipolar cells and 1,309 ganglion cells; displayed as in A–D). The distant visual stimulus enhanced some projections and suppressed others (E). Specifically, signals from slow OFF bipolar cells to ON/OFF ganglion cells were enhanced (G; $p < 0.001$), while those to OFF ganglion cells were suppressed ($p < 0.01$). In contrast, signals from fast OFF bipolar cells were suppressed more frequently than enhanced regardless of the target ganglion cell types ($p < 0.001$). Note the distinct modulation patterns of the bipolar cell projective field by the two different visual stimuli (e.g., $p < 0.001$ for slow OFF bipolar cell projections to ON/OFF ganglion cells; D versus H).

the entire ganglion cell population. As before, we injected current into a single bipolar cell and monitored changes in ganglion cell firing that were time locked to the current injections. The resulting projective field was compared to the projective field measured previously in darkness. This stimulus led to a massive decrease in the strength of projections from bipolar cells (Figures 7A and S5A–S5C), independent of the changes in ganglion cell firing properties driven by the visual stimulation (Figures S5D and S5E). The probability of sign-preserving projections decreased several-fold, and the most distant projections became undetectable (Figure 7B). For every combination of cell types within the bipolar and ganglion cell populations, the mean effect was a weakening of the projection strength (Figures 7D, S5B, and S5C). However, projections from slow bipolar cell types were much less affected than from fast types (Figures 7C, 7D, and S5B). Some individual cell pairs even experienced a moderate strengthening (Figures 7A, 7C, and S5A).

In a complementary experiment, we stimulated an annulus distant from the recording site, using a randomly moving grating. This stimulus did not affect the baseline activity of neurons in the central area—including the source bipolar cell and target ganglion cells nearby—but it did drive neurons in the periphery (Asari and Meister, 2012; Baccus et al., 2008; Geffen et al., 2007; Ölveczky et al., 2003). The resulting effects were more subtle and diverse than under the global stimulus: about 25% of the bipolar cell projections were suppressed, ~10% were enhanced, and the rest remained unaffected (Figures 7E, S5F, and S5H–S5J). The density of projections declined somewhat, but independent of distance (Figure S5H), leaving the spatial range of the projective field unchanged (Figure 7F). On average, the bipolar cell projective field became weaker and sparser for both sign-preserving and -inverting projections (Figure 7F).

Closer examination showed that these effects differed systematically across cell types (Figures 7G, 7H, and S5G). For example, the projections from fast OFF bipolar cells were uniformly suppressed, regardless of the target ganglion cell types. By contrast, the projections from slow OFF bipolar cells were enhanced toward ON/OFF ganglion cells but suppressed toward the other ganglion cell types (Figures 7G, 7H, and S5G). This bipolar cell type thus forms a switching circuit that selectively

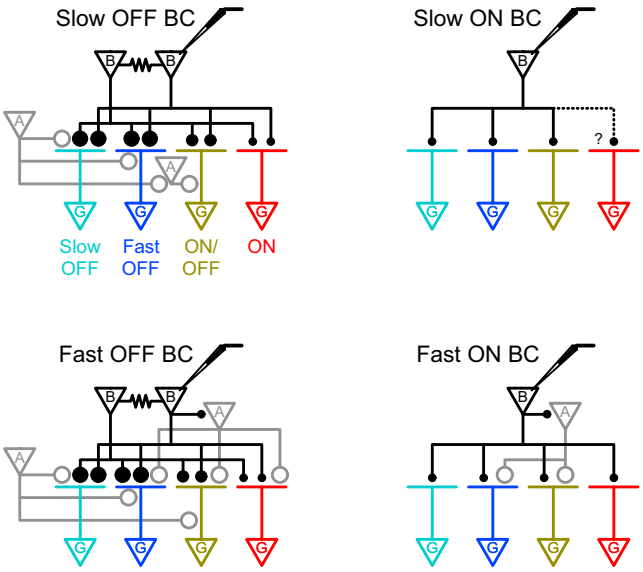

Figure 8. Summary Projection Diagram of the Inner Retina

Schematic diagrams of retinal circuits that serve as working models to summarize and explain the observations. Each panel represents projections from one bipolar cell type to all ganglion cell types. Legend: A, amacrine cell; B, bipolar cell; G, ganglion cell; closed circle, excitatory synapse; open circle, inhibitory synapse; resistor symbol, electrical synapse. OFF bipolar cells (left) make stronger and denser projections (indicated by circle size) to ganglion cells than ON bipolar cells (right). OFF bipolar cells also project signals via electrical synapses. Amacrine cells implement sign-inverting projections, which originate mainly in fast bipolar cell types (bottom). In addition, they carry contextual signals from distant visual stimuli that can modulate the bipolar cell projections in a cell-type-specific fashion (left).

feeds the signals into distinct ganglion cell types under different conditions (Asari and Meister, 2012; Geffen et al., 2007). In turn, this means that the ON/OFF ganglion cell type received a very different mix of bipolar input signals depending on the context of peripheral visual stimulation. These effects may well originate in the interactions with wide-field amacrine cells (Cook and McReynolds, 1998; Geffen et al., 2007; Ölveczky et al., 2003). It appears therefore that the projective field of bipolar cells, like their receptive field, is a dynamic entity, under considerable influence by the context of visual stimulation.

DISCUSSION

In the retina, bipolar cells form the intermediate layer of units interposed between the input neurons and the output neurons. Signals from the photoreceptors converge on a bipolar cell, modulated by the horizontal cell network. From there, the bipolar cell signal diverges to the ganglion cells, modulated by amacrine cell circuits. The convergence of signals from photoreceptors has been documented in great detail, by measuring the bipolar cell receptive field (Fahey and Burkhardt, 2003; Hare and Owen, 1990). By contrast, we aimed at comprehensively addressing the divergence of signals from bipolar to ganglion cells, by measuring the bipolar cell projective field.

Asari and Meister (2012) reported that individual bipolar cells in the salamander retina could evoke distinct responses among ganglion cells, differing in kinetics, adaptation, and rectification properties. The present study gives a comprehensive picture of this signal divergence across the populations of both bipolar and ganglion cells and identifies some systematic rules governing the projections. The major findings are as follows. (1) Signals from individual bipolar cells can spread far into the ganglion cell layer, at least in the quiescent retina without a visual stimulus (Figures 2 and 3). Electrical junctions are partly responsible for this lateral spread (Figure 4). (2) Each functional type of bipolar cell interacts with many different types of ganglion cells (Figure 5). However, the nature of the projection depends substantially on the cell types involved (Figure 6). In particular, cells of opposite response polarity more frequently have projections that are sign-inverting. (3) Fast OFF bipolar cells play a special role: their projections are considerably denser, stronger, and farther reaching than those of other bipolar cell types (Figure 6). (4) Visual stimulation leads to marked changes in the bipolar cell projective field. In general, the influence of individual bipolar cells tends to weaken and shrink in space. However, peripheral motion stimuli also strengthen select projections depending on cell type (Figure 7). In Figure 8, we propose a set of schematics for retinal circuitry that can account for these observations and serves as working models for the underlying mechanisms. In the following, we consider some caveats associated with this approach and interpret the results.

The Relation between Receptive and Projective Fields

The projective field can be understood in close analogy to the more familiar receptive field concept. For example, the receptive field $R(\vec{x},t)$ of a bipolar cell spells out what is the response of the neuron at time t after a brief light flash at location $\vec{x}$. The projective field $P(\vec{y},t)$ spells out what is the response of a ganglion cell at location $\vec{y}$ and time t following a current pulse into the bipolar cell. In the present work, our analysis focused on the spatial profile and the cell-type dependence of the projective field. As regards the temporal dependence, we did observe a wide range of dynamics (Figures 3 and S4), and this topic is discussed further elsewhere (Asari and Meister, 2012).

Since bipolar cells are obligatory interneurons between photoreceptors and ganglion cells, one can view the overall retinal computation as a concatenation of signal convergence onto bipolar cells followed by signal divergence from bipolar cells. If the entire system were linear, one could compute the receptive field of a ganglion cell by simply convolving the receptive and projective fields of bipolar cells:

$$R_G(\vec{x}) = \sum_{\vec{y}} R_B(\vec{x} - \vec{y}) P_B(-\vec{y}). \qquad \text{(Equation 1)}$$

Here $R_G(\vec{x})$ is the ganglion cell receptive field, $R_B(\vec{x})$ is a bipolar cell receptive field, $P_B(\vec{y})$ the bipolar cell projective field, and the sum is over all intervening bipolar cells located at positions $\vec{y}$. Since we measured all the objects in this equation directly (Figure 1), we can test this prediction. Interestingly, it comes out wrong by a good margin: the predicted ganglion cell receptive field, at least for the average case, is much too large (Figures 2D and 2E). Vice versa, if one starts from the measured ganglion cell receptive fields, the inferred bipolar cell

projective field is too small. Clearly the overall function of the retina cannot be treated as a linear system from light to ganglion cell firing. And the nonlinearities seem to effectively shrink the range of influence of a bipolar cell compared to the projective field. Two such effects can be identified already.

First, our projective fields were measured primarily in the dark or under constant uniform illumination (Figures 1 and 6). In that case, the retina is quiet like a smooth pond, which improves the chances of resolving the ripples caused by a single bipolar cell. However, when measuring ganglion cell receptive fields by white-noise analysis, for example, the stimulus is dynamic and the retina becomes active. We found that under visual stimulation the projective field can weaken substantially, and long-range connections are lost (Figure 7). Thus, it is likely that under conditions needed for the receptive field measurement, the bipolar cell projective fields are smaller than we measured in darkness. Indeed, ganglion cell receptive fields measured in the dark with a spot stimulus are generally larger than those measured by a randomly flickering stimulus (Segev et al., 2006; Zhang and Wu, 2010).

Second, the bipolar cell projective field has an antagonistic surround—with sign-inverting projections at long distances—but the surround may be underestimated by the present methods. If the surround is indeed stronger than presently supposed, then the above convolution will predict a smaller ganglion cell receptive field, closer to the observations. What is the evidence for the surround, and why is it underestimated? We found that sign-preserving projections are most frequent at zero radial distance to the ganglion cell and then decline monotonically with distance. By contrast, the sign-inverting projections are most frequent at ~150 μm distance and then decline more gently (Figure 3B). At a certain radius, one thus expects the sign-inverting projections to dominate, but this has been difficult to verify directly. Such a projection must of course pass through an intermediary amacrine cell and that amacrine must be brought to threshold for synaptic transmission by input from the single bipolar cell with current injection. We expect that many such negative projections have remained undetected owing to the nonlinearities of synaptic transmission to and from amacrine cells.

In measuring receptive fields, one encounters a closely related issue. Many retinal ganglion cells have an antagonistic surround in the receptive field. The surround is generally much weaker per unit area than the center, presumably again because the signal must pass through inhibitory interneurons (Croner and Kaplan, 1995). It may be hard to resolve the surround at all if one uses the same small flashes that serve to probe the receptive field center (Chichilnisky and Kalmar, 2002; Pitkow and Meister, 2012). Instead, a popular stimulus to reveal the surround is an annulus that covers a large area at a given distance from the ganglion cell (Cook and McReynolds, 1998; Zhang and Wu, 2010). The corresponding trick in a projective field measurement would be to place a wide annulus of electrodes in a ring surrounding the stimulated bipolar cell, and the average over this large number of projections could more properly resolve weak effects. Whereas this would require custom device manufacturing, the goal may be more readily achieved by large field optical recordings of ganglion cell activity (Briggman and Euler, 2011) surrounding a stimulated bipolar cell.

The Special Role of OFF-type Projections

In most vertebrate retinas, the OFF pathway is stronger than the ON pathway. Within the ganglion cell population, OFF-type cells are more numerous and tend to have smaller receptive fields (Vallerga and Usai, 1986; Segev et al., 2006; Balasubramanian and Sterling, 2009). Even the individual ON/OFF ganglion cells of the salamander retina show a clear bias toward OFF responses (Burkhardt et al., 1998; Geffen et al., 2007). Various explanations have been invoked for this asymmetry. One argument relies on the efficient encoding of natural scenes, which contain more regions of negative than of positive contrast (Balasubramanian and Sterling, 2009). Other lines of reasoning invoke behavioral needs of the animal. For example, salamanders have a strong preference for dark hiding spots (Himstedt, 1967; Roth, 1987). In any case, one is led to wonder where in the retinal circuit this imbalance arises.

Already at the level of bipolar cells, the OFF-type neurons predominate. In the present electrophysiological survey of the salamander retina, we also found a clear excess of OFF bipolar cells (84%), in line with earlier reports (Hare and Owen, 1990; Zhang and Wu, 2009). However, we also discovered a new contribution: the individual OFF bipolar cell is much more effective in driving ganglion cells than an ON bipolar cell (Figures 5, 6, and S4). In particular, the fast OFF bipolar cells—the group with the fastest light responses—systematically had the strongest projections onto ganglion cells. We also showed that electrical connections enhance both the strength and the density of bipolar projections (Figure 4). This may well contribute to the dominance of the OFF pathway, because OFF bipolar cells are coupled more strongly than ON bipolar cells (Zhang and Wu, 2009).

Modulation of the Projective Field by Visual Context

One striking feature of the projective fields that we measured was that each bipolar cell type projected to every ganglion cell type, except for one case in which insufficient data were available for a test (Figure 5). As a caveat, it should be noted that we used a purely physiological definition of cell types, and the visual response properties in the salamander retina tend to show a continuum rather than distinct clusters (Segev et al., 2006). While it is possible that a finer type of definition would reveal more specific projections, the cell pairs with a significant projection strength were distributed broadly all over the space of visual responses (Figure 5A). This broad distribution of bipolar cell signals is a reflection of the anatomical convergence of multiple bipolar cell types onto individual ganglion cells (McGuire et al., 1986), and the substantial crossover connections of multiple amacrine cell pathways (Pang et al., 2007; Werblin, 2010). In the amphibian retina, the inner plexiform layer is less strictly laminated than in the mammalian retina (Toris et al., 1995). This further enables divergence and convergence of bipolar cell signals.

However, the projective field is not a static entity but depends considerably on the state of the retina. The broad projective field measured in darkness sharpened considerably once the retina became visually active (Figure 7). Local stimuli that directly activate the target ganglion cells generally weaken the projective field of any given bipolar cell and restrict its spatial extent. This can be understood by a shunting of the postsynaptic excitatory conductances: once the glutamate from active bipolar cells

opens dendritic conductances on ganglion or amacrine cells, every incremental synaptic current causes a smaller depolarization. Further attenuation of the projective field may come from presynaptic desensitization of the visually driven bipolar cell itself (Burrone and Lagnado, 2000; Singer and Diamond, 2006).

By contrast, stimulation of distant regions of the retina has more varied and specific effects on the projective field. Some projections are strengthened and others weakened (Figure 7). Because of the lateral distances involved, the effects of peripheral stimulation must be transmitted by inhibitory amacrine cells rather than direct excitatory connections. Thus, the enhancement of certain projections is likely the result of disinhibition of a neuron normally under tonic inhibition (Eggers and Lukasiewicz, 2010; Geffen et al., 2007; Manookin et al., 2008; Roska et al., 1998). Furthermore, note that these enhancements are specific to certain bipolar cell types and ganglion cell types. For example, the same ON/OFF ganglion cell may receive a strengthened input from slow OFF bipolar cells but a weakened input from fast OFF bipolar cells. This indicates that the modulation is not applied to the entire presynaptic or postsynaptic neuron but acts specifically on their synaptic connections (Asari and Meister, 2012). Presynaptic disinhibition of a bipolar cell terminal would satisfy these requirements.

In this way, amacrine cell circuits can selectively route information through the inner retina, depending on the context from visual stimulation elsewhere. The full import of such signal switching for retinal computations remains to be understood, and it would be illuminating to observe it under stimuli that occur naturally. Also a deeper exploration of the underlying mechanisms, testing some of the models in Figure 8, will benefit from direct activation of select amacrine cell types (Geffen et al., 2007), perhaps also by optogenetic methods. Such studies gain in importance because responses in higher visual centers are very commonly modulated by stimulation of the "nonclassical" receptive field (Haider et al., 2010; Vinje and Gallant, 2002), and the retinal component of such effects is still poorly defined.

EXPERIMENTAL PROCEDURES

See Supplemental Experimental Procedures for details. The significance level is 0.05 in all analyses unless noted otherwise.

Electrophysiology

Simultaneous intracellular and multielectrode recordings were performed as described previously (Asari and Meister, 2012), following protocols approved by the Institutional Animal Care and Use Committee at Harvard University. Square pulse currents (±500 pA; 1 s each with 2 s intervals) were injected intracellularly into bipolar cells (or amacrine cells) to probe their projections to ganglion cells (see Figure 1 for example).

Receptive Field Analysis

The spatiotemporal receptive fields of the recorded cells (0.4 s window; 0.01 s bin width) were estimated by reverse-correlation methods using randomly flickering checkerboard stimuli (20–100 μm square fields; 100 frames/s; Meister et al., 1994). The spatial profile was characterized by the Gaussian curve fit at the peak latency (see Figures 1A–1D for example), and the distance between cells was measured from their receptive field centers. The size of the receptive field diameter was calculated as twice the mean SD of the long and short axes (Figures 2C and 2D). The temporal profile was examined at the receptive field center for cell-type classification (Figure S3).

Cell-type Classification

Bipolar cells and ganglion cells were physiologically classified into four types each, based on the polarity and kinetics of their visual responses (Geffen et al., 2009). Each cell type was further subdivided by the receptive field size (Figures 5, 6, and S3). Ganglion cells were classified in the same fashion and sorted further by direction selectivity (estimated from the spatiotemporal receptive field by Fourier analysis; Equation S1) or object motion sensitivity (measured from the visual responses to center and surround grating stimuli shifted synchronously or asynchronously; Equation S2; Ölveczky et al., 2003; Baccus et al., 2008).

Projection Strength and Kinetics

For each pair of a bipolar (or amacrine) cell and a ganglion cell, we computed the strength and kinetics of the projection as described previously (Asari and Meister, 2012). Briefly, we first measured the average firing rates across trials for the 1 s periods of bipolar (or amacrine) cell depolarization and hyperpolarization: r_{dep} and r_{hyp}, respectively. The projection strength was defined as the difference of those evoked firing rates, normalized by the magnitude of unrelated changes in the ganglion cell firing rate:

$$\text{Projection strength} = \frac{\text{Net evoked firing rate}}{\text{Pooled standard deviation}} = \frac{r_{dep} - r_{hyp}}{\sqrt{\left(s_{dep}^2 + s_{hyp}^2\right)/2}}. \quad \text{(Equation 2)}$$

Here s_{dep} and s_{hyp} are the SD of the ganglion cell firing rates across trials of bipolar (or amacrine) cell depolarization and hyperpolarization, respectively. This normalization yields a dimensionless number that reflects the relative importance of the response in the target neuron and allows one to compare the projection strength across cell pairs and under different conditions. Several control analyses tested whether the projection strength is affected by changes in the normalization (Figures S1, S2, and S5).

The projection kinetics were characterized by the latency to the peak firing rate evoked by the current injection (Equation S4; Figures 3 and S4).

Projective Field

The projective field of each bipolar cell was characterized by the Gaussian curve fit to the distance dependence of the projection strength to all simultaneously recorded ganglion cells (e.g., Figure 2A; Equation S3). The projective field diameter was measured as twice the SD of the Gaussian envelope (Figures 2C and 2D). A sign test and Kolmogorov-Smirnov test were used to compare the projective and receptive field profiles of the same cell types (Figure 2C) and those across different cell types (Figure 2D), respectively.

Projection Density

The projection density for a certain population of source and target neurons was defined as the fraction of cell pairs whose projection strength was significantly above the noise floor. The spatial extent of bipolar or amacrine projections was estimated by plotting the projection density as a function of distance (e.g., Figures 3B and 3F). A χ^2 test was used to compare the projection density across different cell types (Figure 6) or different conditions (Figures 4 and 7). A sign test was used to examine whether projection strength changes by drug application (100 μM picrotoxin and 1.0 μM strychnine, Figures 4A–4C; 100 μM meclofenamic acid, Figures 4D–4F) or visual stimulation (full-field Gaussian random flicker, Figures 7A–7D; randomly moving gratings excluding 1-mm-diameter circular area centered at the target bipolar cell; Figures 7E–7H). A rank-sum test was used to examine whether the change in projection strength depends on visual contexts (Figure 7).

SUPPLEMENTAL INFORMATION

Supplemental Information includes Supplemental Experimental Procedures and five figures and can be found with this article online at http://dx.doi.org/10.1016/j.neuron.2013.11.029.

AUTHOR CONTRIBUTIONS

H.A. and M.M. designed the study and wrote the manuscript. H.A. performed experiments and analysis.

ACKNOWLEDGMENTS

We gratefully acknowledge Ed Soucy for assistance with experiments. This work was supported by a Postdoctoral Fellowship for Research Abroad from the Japan Society for the Promotion of Science (H.A.) and grants from the U.S. National Institutes of Health (M.M.).

Accepted: November 21, 2013
Published: February 5, 2014

REFERENCES

Arai, I., Tanaka, M., and Tachibana, M. (2010). Active roles of electrically coupled bipolar cell network in the adult retina. J. Neurosci. *30*, 9260–9270.

Asari, H., and Meister, M. (2012). Divergence of visual channels in the inner retina. Nat. Neurosci. *15*, 1581–1589.

Baccus, S.A. (2007). Timing and computation in inner retinal circuitry. Annu. Rev. Physiol. *69*, 271–290.

Baccus, S.A., Ölveczky, B.P., Manu, M., and Meister, M. (2008). A retinal circuit that computes object motion. J. Neurosci. *28*, 6807–6817.

Balasubramanian, V., and Sterling, P. (2009). Receptive fields and functional architecture in the retina. J. Physiol. *587*, 2753–2767.

Briggman, K.L., and Euler, T. (2011). Bulk electroporation and population calcium imaging in the adult mammalian retina. J. Neurophysiol. *105*, 2601–2609.

Burkhardt, D.A., Fahey, P.K., and Sikora, M. (1998). Responses of ganglion cells to contrast steps in the light-adapted retina of the tiger salamander. Vis. Neurosci. *15*, 219–229.

Burrone, J., and Lagnado, L. (2000). Synaptic depression and the kinetics of exocytosis in retinal bipolar cells. J. Neurosci. *20*, 568–578.

Chichilnisky, E.J., and Kalmar, R.S. (2002). Functional asymmetries in ON and OFF ganglion cells of primate retina. J. Neurosci. *22*, 2737–2747.

Cook, J.E., and Becker, D.L. (1995). Gap junctions in the vertebrate retina. Microsc. Res. Tech. *31*, 408–419.

Cook, P.B., and McReynolds, J.S. (1998). Lateral inhibition in the inner retina is important for spatial tuning of ganglion cells. Nat. Neurosci. *1*, 714–719.

Croner, L.J., and Kaplan, E. (1995). Receptive fields of P and M ganglion cells across the primate retina. Vision Res. *35*, 7–24.

de Vries, S.E.J., Baccus, S.A., and Meister, M. (2011). The projective field of a retinal amacrine cell. J. Neurosci. *31*, 8595–8604.

Doi, E., Gauthier, J.L., Field, G.D., Shlens, J., Sher, A., Greschner, M., Machado, T.A., Jepson, L.H., Mathieson, K., Gunning, D.E., et al. (2012). Efficient coding of spatial information in the primate retina. J. Neurosci. *32*, 16256–16264.

Dong, C.J., and Werblin, F.S. (1998). Temporal contrast enhancement via $GABA_C$ feedback at bipolar terminals in the tiger salamander retina. J. Neurophysiol. *79*, 2171–2180.

Eggers, E.D., and Lukasiewicz, P.D. (2010). Interneuron circuits tune inhibition in retinal bipolar cells. J. Neurophysiol. *103*, 25–37.

Fahey, P.K., and Burkhardt, D.A. (2003). Center-surround organization in bipolar cells: symmetry for opposing contrasts. Vis. Neurosci. *20*, 1–10.

Field, G.D., Gauthier, J.L., Sher, A., Greschner, M., Machado, T.A., Jepson, L.H., Shlens, J., Gunning, D.E., Mathieson, K., Dabrowski, W., et al. (2010). Functional connectivity in the retina at the resolution of photoreceptors. Nature *467*, 673–677.

Geffen, M.N., de Vries, S.E.J., and Meister, M. (2007). Retinal ganglion cells can rapidly change polarity from Off to On. PLoS Biol. *5*, e65.

Geffen, M.N., Broome, B.M., Laurent, G., and Meister, M. (2009). Neural encoding of rapidly fluctuating odors. Neuron *61*, 570–586.

Gollisch, T., and Meister, M. (2010). Eye smarter than scientists believed: neural computations in circuits of the retina. Neuron *65*, 150–164.

Haider, B., Krause, M.R., Duque, A., Yu, Y., Touryan, J., Mazer, J.A., and McCormick, D.A. (2010). Synaptic and network mechanisms of sparse and reliable visual cortical activity during nonclassical receptive field stimulation. Neuron *65*, 107–121.

Hare, W.A., and Owen, W.G. (1990). Spatial organization of the bipolar cell's receptive field in the retina of the tiger salamander. J. Physiol. *421*, 223–245.

Hare, W.A., and Owen, W.G. (1996). Receptive field of the retinal bipolar cell: a pharmacological study in the tiger salamander. J. Neurophysiol. *76*, 2005–2019.

Himstedt, W. (1967). Experimentelle Analyse der optischen Sinnesleistungen im Beutefangverhalten der einheimischen Urodelen. Zool. Jahrb. Physiol. *73*, 281–320.

Lehky, S.R., and Sejnowski, T.J. (1988). Network model of shape-from-shading: neural function arises from both receptive and projective fields. Nature *333*, 452–454.

Manookin, M.B., Beaudoin, D.L., Ernst, Z.R., Flagel, L.J., and Demb, J.B. (2008). Disinhibition combines with excitation to extend the operating range of the OFF visual pathway in daylight. J. Neurosci. *28*, 4136–4150.

Masland, R.H. (2012). The neuronal organization of the retina. Neuron *76*, 266–280.

McGuire, B.A., Stevens, J.K., and Sterling, P. (1984). Microcircuitry of bipolar cells in cat retina. J. Neurosci. *4*, 2920–2938.

McGuire, B.A., Stevens, J.K., and Sterling, P. (1986). Microcircuitry of beta ganglion cells in cat retina. J. Neurosci. *6*, 907–918.

Meister, M., Pine, J., and Baylor, D.A. (1994). Multi-neuronal signals from the retina: acquisition and analysis. J. Neurosci. Methods *51*, 95–106.

Münch, T.A., da Silveira, R.A., Siegert, S., Viney, T.J., Awatramani, G.B., and Roska, B. (2009). Approach sensitivity in the retina processed by a multifunctional neural circuit. Nat. Neurosci. *12*, 1308–1316.

Nirenberg, S., and Meister, M. (1997). The light response of retinal ganglion cells is truncated by a displaced amacrine circuit. Neuron *18*, 637–650.

Ölveczky, B.P., Baccus, S.A., and Meister, M. (2003). Segregation of object and background motion in the retina. Nature *423*, 401–408.

Pang, J.-J., Gao, F., and Wu, S.M. (2004). Stratum-by-stratum projection of light response attributes by retinal bipolar cells of *Ambystoma*. J. Physiol. *558*, 249–262.

Pang, J.-J., Gao, F., and Wu, S.M. (2007). Cross-talk between ON and OFF channels in the salamander retina: indirect bipolar cell inputs to ON-OFF ganglion cells. Vision Res. *47*, 384–392.

Pitkow, X., and Meister, M. (2012). Decorrelation and efficient coding by retinal ganglion cells. Nat. Neurosci. *15*, 628–635.

Roska, B., and Werblin, F. (2001). Vertical interactions across ten parallel, stacked representations in the mammalian retina. Nature *410*, 583–587.

Roska, B., Nemeth, E., and Werblin, F.S. (1998). Response to change is facilitated by a three-neuron disinhibitory pathway in the tiger salamander retina. J. Neurosci. *18*, 3451–3459.

Roth, G. (1987). Visual Behavior in Salamanders. (Berlin: Springer-Verlag).

Segev, R., Puchalla, J., and Berry, M.J., 2nd. (2006). Functional organization of ganglion cells in the salamander retina. J. Neurophysiol. *95*, 2277–2292.

Siegert, S., Scherf, B.G., Del Punta, K., Didkovsky, N., Heintz, N., and Roska, B. (2009). Genetic address book for retinal cell types. Nat. Neurosci. *12*, 1197–1204.

Singer, J.H., and Diamond, J.S. (2006). Vesicle depletion and synaptic depression at a mammalian ribbon synapse. J. Neurophysiol. *95*, 3191–3198.

Tachibana, M., and Kaneko, A. (1988). Retinal bipolar cells receive negative feedback input from GABAergic amacrine cells. Vis. Neurosci. *1*, 297–305.

Toris, C.B., Eiesland, J.L., and Miller, R.F. (1995). Morphology of ganglion cells in the neotenous tiger salamander retina. J. Comp. Neurol. *352*, 535–559.

Vallerga, S., and Usai, C. (1986). Relation between light responses and dendritic branching in the salamander ganglion cells. Exp. Biol. *45*, 81–90.

Vaney, D.I. (1991). Many diverse types of retinal neurons show tracer coupling when injected with biocytin or Neurobiotin. Neurosci. Lett. *125*, 187–190.

Vaney, D.I., Sivyer, B., and Taylor, W.R. (2012). Direction selectivity in the retina: symmetry and asymmetry in structure and function. Nat. Rev. Neurosci. *13*, 194–208.

Vinje, W.E., and Gallant, J.L. (2002). Natural stimulation of the nonclassical receptive field increases information transmission efficiency in V1. J. Neurosci. *22*, 2904–2915.

Völgyi, B., Chheda, S., and Bloomfield, S.A. (2009). Tracer coupling patterns of the ganglion cell subtypes in the mouse retina. J. Comp. Neurol. *512*, 664–687.

Wässle, H., Puller, C., Müller, F., and Haverkamp, S. (2009). Cone contacts, mosaics, and territories of bipolar cells in the mouse retina. J. Neurosci. *29*, 106–117.

Werblin, F.S. (1970). Response of retinal cells to moving spots: intracellular recording in Necturus maculosus. J. Neurophysiol. *33*, 342–350.

Werblin, F.S. (2010). Six different roles for crossover inhibition in the retina: correcting the nonlinearities of synaptic transmission. Vis. Neurosci. *27*, 1–8.

Wong-Riley, M.T. (1974). Synaptic orgnization of the inner plexiform layer in the retina of the tiger salamander. J. Neurocytol. *3*, 1–33.

Wu, S.M. (1994). Synaptic transmission in the outer retina. Annu. Rev. Physiol. *56*, 141–168.

Wu, S.M., Gao, F., and Maple, B.R. (2000). Functional architecture of synapses in the inner retina: segregation of visual signals by stratification of bipolar cell axon terminals. J. Neurosci. *20*, 4462–4470.

Yang, C.Y., and Wang, H.H. (1999). Anatomical and electrophysiological evidence for GABAergic bipolar cells in tiger salamander retina. Vision Res. *39*, 3653–3661.

Zhang, A.-J., and Wu, S.M. (2009). Receptive fields of retinal bipolar cells are mediated by heterogeneous synaptic circuitry. J. Neurosci. *29*, 789–797.

Zhang, A.-J., and Wu, S.M. (2010). Responses and receptive fields of amacrine cells and ganglion cells in the salamander retina. Vision Res. *50*, 614–622.

Neuron, Volume *81*

Supplemental Information

The Projective Field of Retinal Bipolar Cells and Its Modulation by Visual Context

Hiroki Asari and Markus Meister

Inventory of supplemental information

- Supplemental data:
  - Figure S1, related to Figure 3.
  - Figure S2, related to Figure 4.
  - Figures S3 and S4, related to Figures 5 and 6.
  - Figure S5, related to Figure 7.
- Supplemental experimental procedures.
- Supplemental references.

Supplemental data

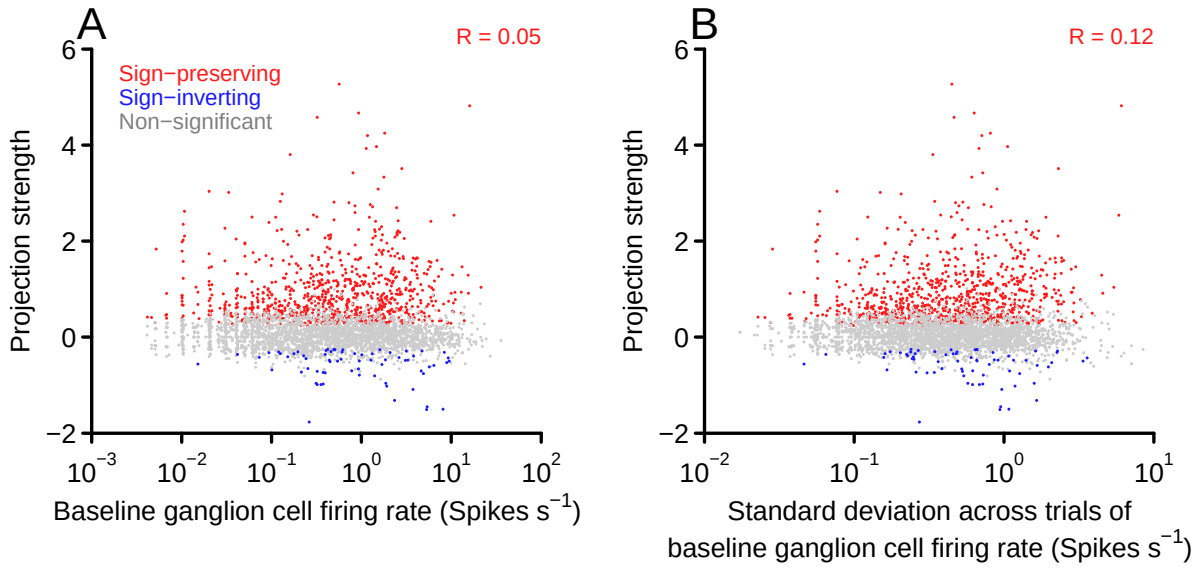

Figure S1: Projection strength is not correlated with the baseline firing rate of ganglion cells or its variability across trials, related to Figure 3.

The projection strength is defined as a ratio of evoked changes in firing rate, normalized by unrelated changes in the firing rate (Eq.(2)). Here we test whether the resulting ratio is systematically influenced by the normalization factor.

(A) Population data of the projection strength (red, significant sign-preserving; blue, significant sign-inverting; gray, non-significant) as a function of the baseline firing rate of ganglion cells. Correlation coefficient for sign-preserving projections (R) is displayed on the top-right corner.

(B) Population data of the projection strength as a function of the variability of baseline ganglion cell firing rate, measured as the standard deviation across trials (displayed as in panel A).

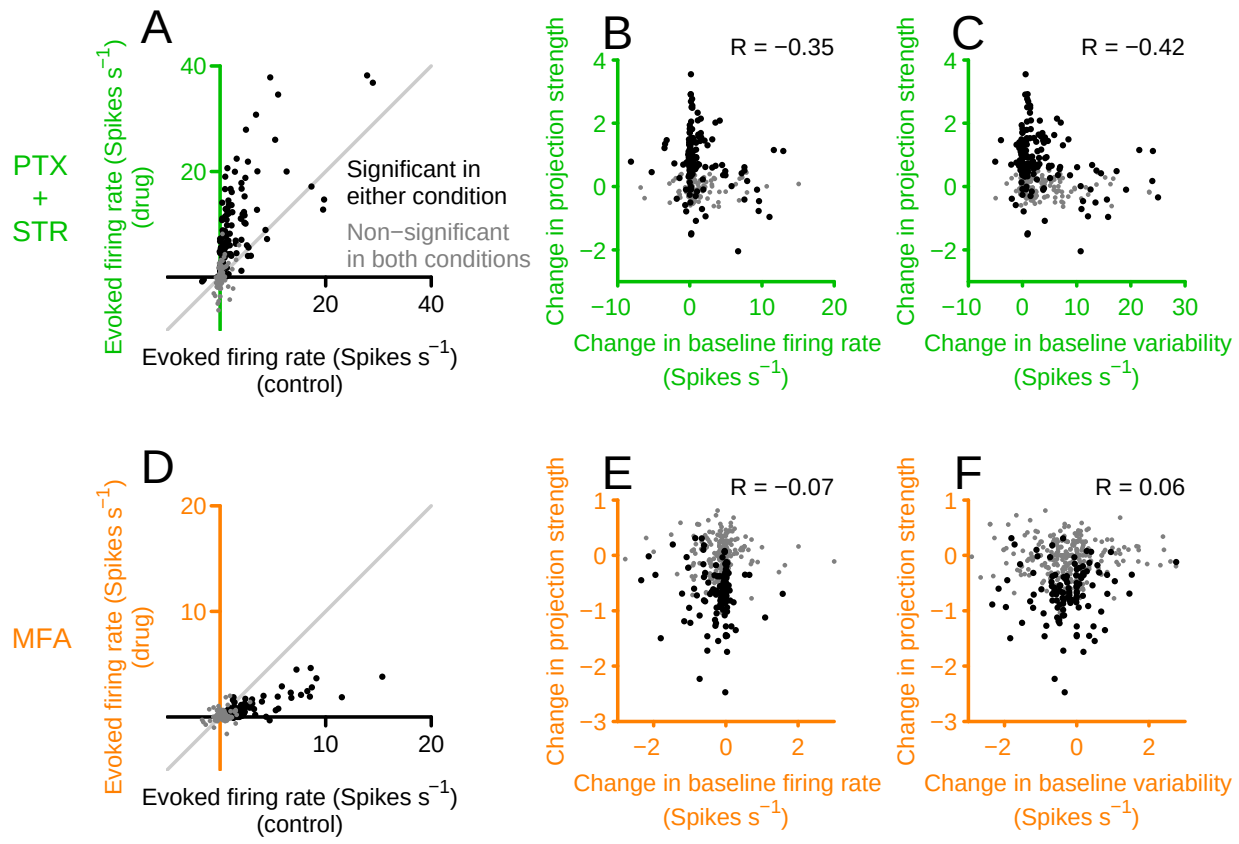

Figure S2: Change in projection strength by drug application is not correlated with change in baseline ganglion cell firing rate or its variability across trials, related to Figure 4.

(A, D) Net evoked firing rate of ganglion cells in response to bipolar cell current injections before and after applying picrotoxin and strychnine (A; PTX+STR) or meclofenamic acid (D; MFA): black, significant projection in at least one condition; gray, non-significant in both conditions. Displayed as in Figures 4A and 4D, respectively.

(B, C, E, F) Change in bipolar cell projection strength by the drug application (B, C: picrotoxin and strychnine; E, F: meclofenamic acid) as a function of the changes in baseline ganglion cell firing rate (B, E) or its variability, measured as the standard deviation across trials (C, F). Correlation coefficient for significant projections (R) is displayed on the top-right corner of each panel.

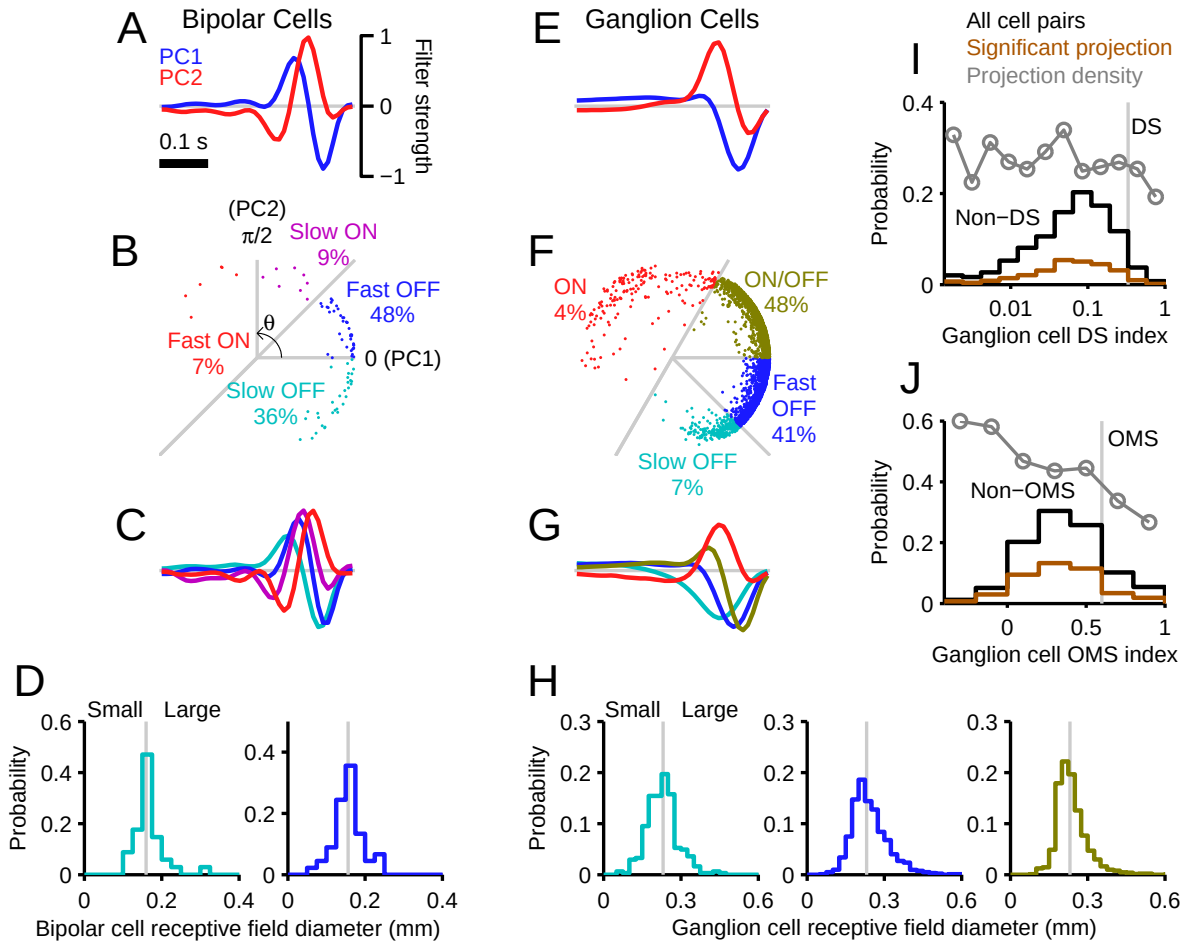

Figure S3: Cell type classification, related to Figures 5 and 6.

(A–D) To physiologically classify bipolar cell types, we performed principal component analysis on their temporal filters (A) and projected them onto the two-dimensional space spanned by the first two principal components (PC1 and PC2; $N = 86$ cells; B). Based on the angle θ around the origin in this space (0, PC1; $\pi/2$, PC2; boundaries in gray lines; B), we grouped the temporal filters into four subtypes (mean filters color-coded in panel C; same scale as in panel A). The Slow OFF (cyan) and Fast OFF (blue) cell types were further divided into Small and Large types based on the receptive field diameters (D; boundary in gray at the median).

(E–H) Ganglion cells were classified by the same methods into four subtypes from the temporal filters ($N = 4{,}236$ cells; E–G) with a finer subdivision by the receptive field size (except for the ON cell type; H). Displayed as in panels A–D.

(I) Ganglion cell direction selectivity (DS) index was calculated from the spatiotemporal receptive field by Fourier analysis (from Eq.(S1); black, all data; brown, significant projection) for classifying DS and Non-DS cells (boundary in gray vertical line). Bipolar cell projection density (gray) was not dependent on the DS index (slope, -0.02 ± 0.03; y-intercept, 0.24 ± 0.05; linear regression with 95% confidence interval).

(J) Object motion sensitivity (OMS) index was calculated for a subset of ganglion cells (within 0.35 mm from target bipolar cells; $N = 845$) from their responses to a grating stimulus with global and differential motion between center region (1-mm-diameter circular area centered at the target bipolar cells) and the surround region (Eq.(S2)). Bipolar cell projection was observed less frequently to OMS ganglion cells (slope, -0.27 ± 0.07; y-intercept, 0.53 ± 0.04). Displayed as in panel I.

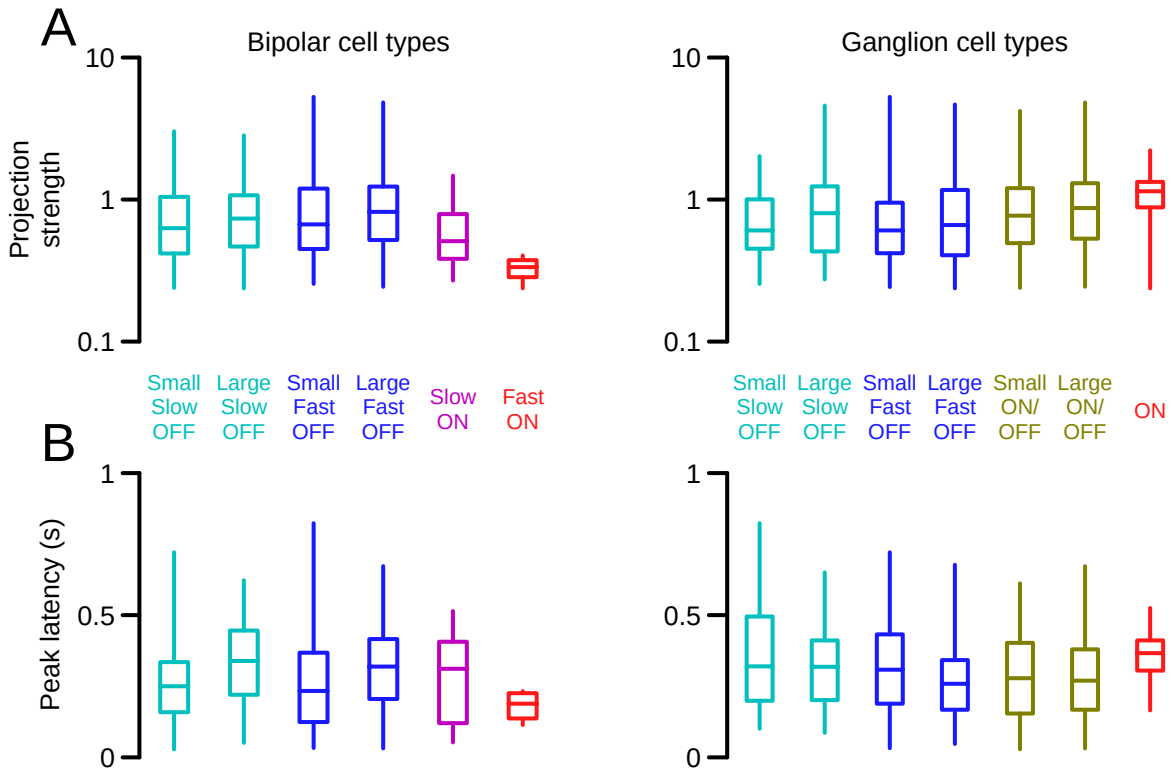

Figure S4: Projection strength and peak latency across different cell types, related to Figures 5 and 6.

(A) Projection strength across different cell types. The data were sorted by projections from distinct bipolar cell types (left), or by projections to distinct ganglion cell types (right). The box plot represents the minimum, first quartile, median, third quartile, and maximum values of the projection strength for the cell pairs with significant sign-preserving projection in each category. Note logarithmic axis.

(B) Peak latency of ganglion cell responses to bipolar cell depolarization (left, across bipolar cell types; right, across ganglion cell types; displayed as in panel A).

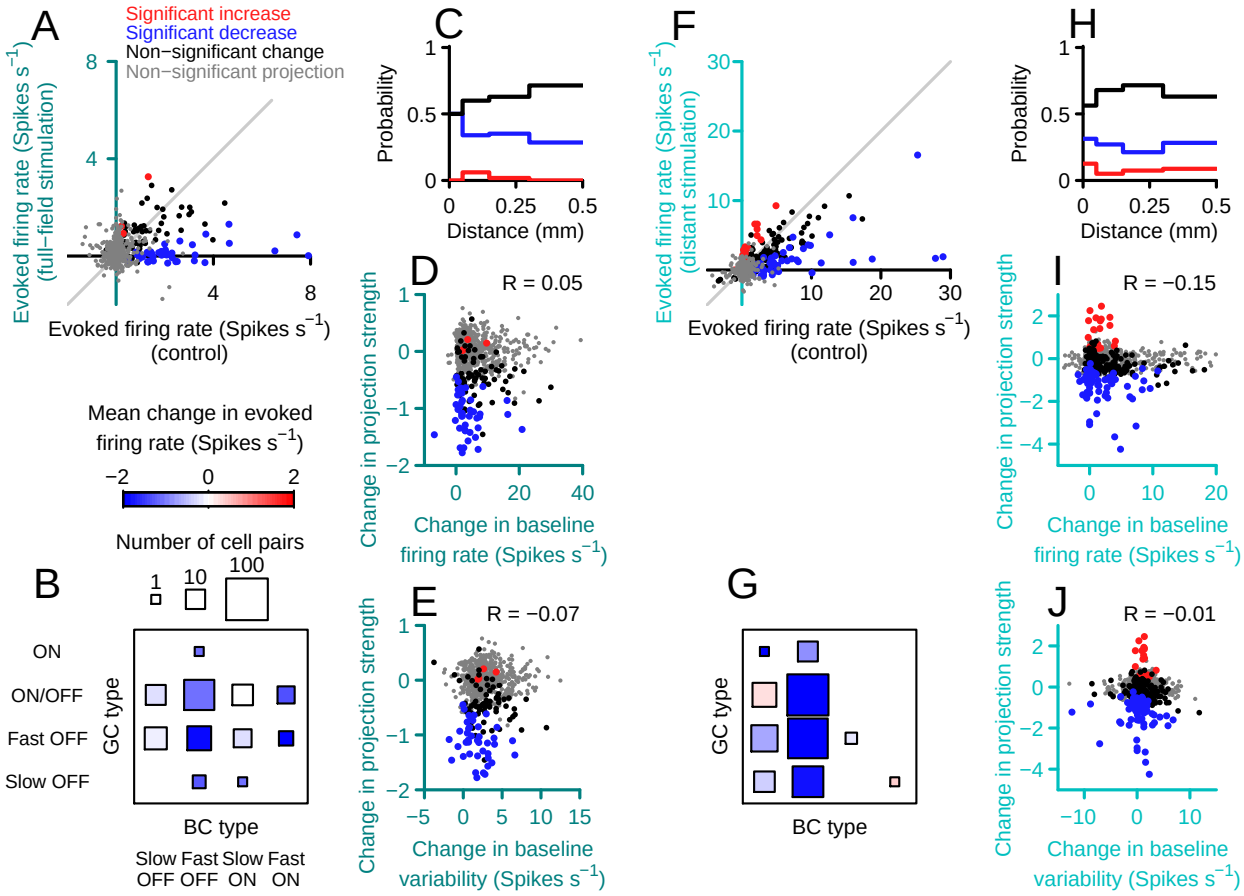

Figure S5: Change in projection strength by visual stimulation is not correlated with change in baseline ganglion cell firing rate or its variability across trials, related to Figure 7.

(A) Net evoked firing rate of ganglion cells by bipolar cell current injection in the presence and absence of full-field visual stimulation (gray, non-significant projection in both conditions; black, red, and blue, significant projection in at least one condition; red, significant increase during visual stimulation; blue, significant decrease). Displayed as in Figure 7A.

(B) Mean change in the net evoked firing rate among distinct pairs of bipolar and ganglion cell types (red hue, positive; blue hue, negative; displayed as in Figure 7D).

(C) Fraction of cell pairs with significant projection that showed significant increase (red) or decrease (blue) in the projection strength by the visual stimulation (black, non-significant change), plotted against the distance between the cells.

(D, E) Change in bipolar cell projection strength by the full-field visual stimulation as a function of the changes in baseline ganglion cell firing rate (D) or its variability, measured as the standard deviation across trials (E). Correlation coefficient for significant projections (R) is displayed on the top-right corner of each panel.

(F–J) Same analysis for the effects of distant visual stimulation (displayed as in panels A–E, respectively).

Supplemental experimental procedures

Electrophysiology

The dark-adapted retina of a larval tiger salamander (*Ambystoma tigrinum*) was isolated and placed on a flat array of 61 extracellular electrodes with the ganglion cell side down (Meister et al., 1994). The retina was superfused with oxygenated Ringer's medium (in mM: NaCl, 110; $NaHCO_3$, 22; KCl, 2.5; $MgCl_2$, 1.6; $CaCl_2$, 1; and D-glucose, 10; equilibrated with 95% O_2 and 5% CO_2 gas) at room temperature. Sharp intracellular microelectrodes were filled with 2 M potassium acetate and 3% Rhodamine Dextran 10,000 MW (fluorescent dye; Molecular Probes) with a final impedance of 150-250 MΩ, and blindly inserted into various cells until one with the visual response characteristics matching those of bipolar cells or amacrine cells was found (Baccus and Meister, 2002). We used an Axoclamp 2B amplifier (Molecular Devices) in bridge mode to monitor membrane potential and deliver command signals into individual cells. Specifically, we alternately delivered depolarizing and hyperpolarizing square pulse currents (500 pA; 1 s each) into cells with 2 s intervals (see Figure 1). Depolarization of the bipolar cell by the current injection was not significantly different among the bipolar cell types (ON, 29.4 ± 5.6 mV; OFF, 40.5 ± 4.5 mV; mean $\pm$ standard error; $p > 0.39$, rank sum test). To test whether this current injection somehow depolarizes ganglion cells directly, we injected current into the extracellular space between neurons and found no resulting activity in ganglion cells. Furthermore, current injection into amacrine cells was found to inhibit ganglion cells (Figures 2B and 3E). For additional control experiments, see Asari and Meister (2012).

In total, recordings were made from 86 bipolar cells together with 4,236 ganglion cells, and from 10 amacrine cells with 347 ganglion cells. To study interactions with the surrounding circuits, 10 bipolar cells were examined with 100 μM picrotoxin and 1.0 μM strychnine, and 8 bipolar cells with 100 μM meclofenamic acid (Figures 4 and S2). These drugs were also applied during 5 amacrine cell recordings (Figure 4B and E). Because washout of these drugs from a whole-mount preparation is slow (Cook et al., 2000; Veruki and Hartveit, 2009), we could not achieve full reversal of the drug effects within the available time—typically, half an hour for the intracellular recordings. Thus we only compared measurements before and after drug application, with no analysis of the washout. To study visual context-dependence of bipolar cell projective fields, 27 bipolar cells were examined in the presence of distant visual stimuli, and 15 bipolar cells under full-field visual stimulation (Figures 7 and S5).

Visual stimulation

Visual stimuli were displayed on a gamma-corrected cathode-ray tube monitor (DELL E773c; frame rate 100 Hz; mean luminance 18 mW/m^2) and projected onto the photoreceptor layer of the retina. We used the following four sets of visual stimuli, although not all stimuli were presented to all cells.

1. To identify the cells penetrated by the sharp electrodes, we examined their responses to a flashing center spot (200 μm diameter), annulus ring (500 μm inner diameter; 1,000 μm outer diameter), or uniform field.

2. To map the spatio-temporal receptive fields of all recorded cells (see Figure 1A–D for example), we presented randomly flickering checkerboard stimuli for 10-15 minutes (20-100 μm square fields; Meister et al., 1994).

3. To examine the visual context-dependence of bipolar cell projective fields (Figures 7 and S5), we presented full-field random flicker (100 frames per second; intensity drawn from Gaussian distribution with mean luminance of 18 mW/m^2 and standard deviation of 7 mW/m^2) while injecting current into the target bipolar cell.

4. To examine interactions between a bipolar cell and its surrounding circuitry (Figures 7 and S5), we covered the entire visual field (6,400$\times$4,800 μm) with a grating of black and white stripes (80 μm width), and divided it into a circular center region (1,000 μm in diameter, centered at the bipolar cell soma) and the surrounding background region. In combination with the current injection into the bipolar cell, the surrounding grating was then either shifted by a half period every 200 ms or jittered on every 10 ms frame update (Gaussian random motion with a standard deviation of 2 mm$/$s, corresponding to a step size of 2 pixels$/$frame) to recruit inputs from wide-field amacrine cells (Baccus et al., 2008; Geffen et al., 2007). In the former shifting case, every current injection trial was delayed by 50 ms to vary the relative timing between the onset of square pulse currents and that of background stimulus motion. The center region remained static so as not to visually stimulate the current-stimulated bipolar cell or nearby ganglion cells (Asari and Meister, 2012). To examine object motion sensitivity of ganglion cells (Figures 5E and 6D), these center and surround regions were shifted in sync or out of sync at 0.5 Hz without bipolar cell current injection (Baccus et al., 2008; Ölveczky et al., 2003).

Data analysis

For extracellular recordings, spike trains from individual ganglion cells were extracted from raw voltage traces by a semi-automated spike-sorting algorithm written in Igor (Wave Metrics; Pouzat et al., 2002). Although the ganglion cell layer contains some displaced amacrine cells as well, their action potentials are expected to be below the noise level of the multielectrode recordings and are attenuated further by signal filtering prior to spike sorting (Segev et al., 2004). The extracted spike timing data and intracellular data traces were then analyzed in Matlab (Mathworks). The significance level is 0.05 in all analyses except where noted otherwise.

Receptive field analysis

The spatio-temporal receptive fields of the recorded cells were estimated by reverse-correlation methods (Meister et al., 1994). Using the random flicker stimulus, we computed the response-weighted average of the stimulus waveform (0.4 s window; 0.01 s bin width), where the weight is the measured membrane voltage for bipolar cells (Figure 1A) or amacrine cells, and spike number for ganglion cells (Figure 1C, D). To characterize the receptive field structures, we computed two-dimensional Gaussian fits to the spatial receptive field at the peak latency. The location of the cell was then assigned to the center of that Gaussian profile (Figure 1B), and the size of the receptive field diameter was estimated as twice the mean standard deviation of the long and short axes (Figure 2C, D).

Cell-type classification

The five major classes of retinal neurons can be recognized unambiguously by online analysis. Within each class, cells show a wide range of anatomical and physiological properties (Awatramani and Slaughter, 2000; DeVries, 2000; Masland, 2012; Wu et al., 2000). In this study, the need for simultaneous recording prohibited a morphological analysis of individual neurons. Specifically, because we serially impaled multiple cells in each retina with sharp electrodes, we failed to identify the exact target cells after recordings. We thus focused on visual response properties for cell type classification (Figure S3; see also Geffen et al., 2009). First we performed a principal component analysis on the temporal filters derived from receptive field analysis of all bipolar or ganglion cells (Figure S3A and D, respectively). The first two principal components (PC1 and PC2) were largely sufficient to fit all the waveform shapes, accounting for 78% of the total variance

for bipolar cells (Figure S3B) and 77% for ganglion cells (Figure S3E). Each waveform is a point in the two-dimensional space spanned by PC1 and PC2, and we characterized its shape by the angle around the origin, $\theta \in (-\pi, \pi]$, with $\theta = 0$ for PC1 and $\theta = \pi/2$ for PC2. Finally, based on this angle θ, we grouped bipolar and ganglion cells into four subtypes each. For bipolar cells, the boundaries for the four subtypes (Slow OFF, Fast OFF, Slow ON, and Fast ON bipolar cell types) were set to be $-3\pi/4$, 0, $\pi/4$, and $\pi/2$ (Figure S3C). For ganglion cells, the boundaries were set to be $-2\pi/3$, $-\pi/4$, 0, and $\pi/3$, corresponding to the Slow OFF, Fast OFF, ON/OFF, and ON ganglion cell types, respectively (Figure S3F).

For the salamander retina, cells in this feature space tend to form a continuum rather than breaking naturally into discrete clusters (Figure S3B, E; Segev et al., 2006). Any of the subtypes we defined might thus contain several cell types if classified by different criteria. Here we made a finer cell-type classification in the following three ways. Note that ON cell types were excluded from this refined analysis due to scarcity of the data.

1. We subdivided each of the bipolar and ganglion cell types based on the receptive field size (boundary at the median; Figure S3D and H, respectively).

2. We classified ganglion cells into direction selective and non-selective types (Vaney et al., 2012). Ganglion cell direction selectivity was estimated from the spatiotemporal receptive field, $R(\mathbf{x}, t)$, where $\mathbf{x}$ and t represent space and time, respectively. Specifically, we first Fourier transformed $R(\mathbf{x}, t)$ to represent the receptive field in the frequency domain: $\widehat{R}(\boldsymbol{\omega}, \xi) = \mathcal{F}[R(\mathbf{x}, t)]$. Here $\boldsymbol{\omega}$ and ξ are spatial and temporal frequency, respectively; and $\mathcal{F}[\cdot]$ is the three-dimensional Fourier transform. We then identified the frequencies $(\boldsymbol{\omega}_{\text{max}} \neq 0, \xi_{\text{max}} \neq 0)$ where the amplitude spectrum $|\widehat{R}(\boldsymbol{\omega}, \xi)|$ was maximal, and introduced a direction-selectivity (DS) index as follows:

$$\text{DS index} = \frac{|\widehat{R}(\boldsymbol{\omega}_{\text{max}}, \xi_{\text{max}})| - |\widehat{R}(\boldsymbol{\omega}_{\text{max}}, -\xi_{\text{max}})|}{|\widehat{R}(\boldsymbol{\omega}_{\text{max}}, \xi_{\text{max}})| + |\widehat{R}(\boldsymbol{\omega}_{\text{max}}, -\xi_{\text{max}})|}. \tag{S1}$$

   Note that $|\widehat{R}(\boldsymbol{\omega}_{\text{max}}, \xi_{\text{max}})|$ and $|\widehat{R}(\boldsymbol{\omega}_{\text{max}}, -\xi_{\text{max}})|$ represent the linear estimate of the ganglion cell response to a grating stimulus moving in preferred and null direction, respectively. We classified a ganglion cell as direction selective if $|\widehat{R}(\boldsymbol{\omega}_{\text{max}}, \xi_{\text{max}})| \geq 2|\widehat{R}(\boldsymbol{\omega}_{\text{max}}, -\xi_{\text{max}})|$, that is, DS index $\geq 1/3$ (Figure S3I).

3. We sorted ganglion cells into object motion sensitive and non-sensitive groups (Baccus et al., 2008; Ölveczky et al., 2003). In a subset of our recordings, we presented a grating stimulus and shifted either the entire grating rigidly ("global") or the center and surround regions at different times ("differential"). Based on the firing responses to these two stimuli, r_{global} and r_{diff}, respectively, we then introduced an index for the object motion sensitivity (OMS):

$$\text{OMS index} = \frac{r_{\text{diff}} - r_{\text{global}}}{r_{\text{diff}} + r_{\text{global}}}. \tag{S2}$$

Because the circular center region (1 mm diameter) was centered at the impaled bipolar cells but not at individual ganglion cells, here we excluded those ganglion cells outside the anatomically expected range of monosynaptic transmission (0.35 mm; Pang et al., 2004; Wu et al., 2000; Zhang and Wu, 2009, 2010). We classified a ganglion cell as object motion sensitive if $r_{\text{diff}} \geq 4r_{\text{global}}$, that is, OMS index ≥ 0.6 (Figure S3J).

Projective field analysis

We used the following methods to identify the projection from upstream bipolar (or amacrine) cells to downstream ganglion cells and estimate the projective field. For each target neuron, we measured the strength of the projection and its kinetics. First, we computed the peri-stimulus time histogram (0.1 s bin width) of ganglion cell spiking activity while injecting current into a bipolar (or amacrine) cell intracellularly. For those ganglion cells that showed significantly different firing rates from their baseline activity r_{base} (1 s period before the onset of the current injection) in at least one bin during the current injection periods (two-tailed *t*-test with Bonferroni correction), we calculated the average firing rates across trials for the 1-s periods of bipolar (or amacrine) cell depolarization and hyperpolarization: r_{dep} and r_{hyp}, respectively. If the net evoked firing rate, $r = r_{\text{dep}} - r_{\text{hyp}}$, was significantly above or below zero, then we considered that the bipolar (or amacrine) cell carried sign-preserving or sign-inverting signals to the ganglion cell, respectively. Confidence intervals were estimated by bootstrap resampling methods over trials (10,000 repeats).

The noise floor was estimated by resampling methods where spike timings were randomly shifted to neutralize the temporal correlation to the onset of the current injection, followed by the same significance

tests described above. For each cell, we repeated this procedure 1,000 times, and took the average over the population to calculate the level of false positives in the analysis (e.g., $p = 0.006$ in Figure 3B).

The spatial extent of bipolar (or amacrine) cell signals was then estimated by the probability of having a significant projection above the noise floor as a function of distance (Z-test with Bonferroni correction; Figures 3, 4, and 7). This is a conservative estimate of connection probability, because statistical significance is limited by the finite data length, and because we measured spiking activity of ganglion cells but not their subthreshold responses. Nevertheless, the estimate is not biased and thus supports a statistical comparison (χ^2-test) across different cell types (Figure 6) or different conditions (Figures 4 and 7). The dominance of OFF cell types over ON types in the salamander retina (Segev et al., 2006; Vallerga and Usai, 1986), however, poses a limitation on the analysis across distinct cell types (Figures 5, 6, and S3). For example, we rarely observed significant projection from ON bipolar cells to ON ganglion cells (1 out of 44 cell pairs; Figure 5A, B). This was significantly less than the projection between OFF bipolar cells and ON ganglion cells (28 out of 149 cell pairs; $p = 0.007$, proportion test), but not between ON bipolar cells and ON/OFF ganglion cells (34 out of 418 cell pairs; $p > 0.16$). The scarcity of the projection between ON cell types is thus most likely due to lack of data, but not the absence of the projections.

To quantify the projection strength of individual cell pairs regardless of the significance from the above analysis, we used the following definition (Asari and Meister, 2012):

$$\text{Projection strength} = \frac{\text{Net evoked firing rate}}{\text{Pooled standard deviation}} = \frac{r_{\text{dep}} - r_{\text{hyp}}}{\sqrt{(s_{\text{dep}}^2 + s_{\text{hyp}}^2)/2}}, \qquad \text{(2; revisited)}$$

where s_{dep} and s_{hyp} are the standard deviation of the ganglion cell firing rates across trials of bipolar (or amacrine) cell depolarization and hyperpolarization, respectively. This standardized measure does not depend on the data length (number of trials), unlike the p-values in the significance tests. The observed projection strength or its change were not correlated with the baseline firing property of ganglion cells or its change under different conditions (Figures S1, S2, and S5). Confidence intervals were estimated by the bootstrap resampling methods over trials (10,000 repeats; e.g., Figure 2A).

We used a Gaussian fit $g(x)$ to characterize the projection strength as a function of distance x between cell pairs:

$$g(x) = a \exp\left[-\frac{x^2}{2b^2}\right], \qquad \text{(S3)}$$

where a and b are the amplitude and radius of the Gaussian envelope, respectively (Figure 2). The projective field diameter was measured as $2b$.

To characterize the projection dynamics, we first fitted the following unimodal function $f(t)$ to the peri-stimulus time histogram of ganglion cell responses under current stimulation of a bipolar or amacrine cell (Asari and Meister, 2012):

$$f(t) = \alpha t^{\beta} \exp\left[-\frac{t}{\gamma}\right] + r_{\text{base}}, \tag{S4}$$

where α, β, and γ denote the free parameters, and t (> 0) indicates the time after the onset of current injection. The peak latency was then computed as $t_{\text{peak}} = \beta\gamma$ and the peak evoked firing rate as $r_{\text{peak}} = f(t_{\text{peak}}) - r_{\text{base}}$. For those projections with $r_{\text{peak}} > 1$ spike/s, we calculated the pairwise correlation coefficients among t_{peak}, the projection strength, and the distance between the cells (Figures 3 and 6) with p-values for testing the hypothesis of no correlation.

Linear analysis of receptive and projective fields

In Figure 2E, the measured bipolar and ganglion cell receptive fields were computed by averaging the spatial filters over the respective population. The measured bipolar cell projective field was acquired by pooling the projection profile (e.g., Figure 2A) over all bipolar cells and smoothing by local linear regression spanning 20% of the data. From Eq.(1), the predicted ganglion cell receptive field was then obtained by the linear convolution of the measured bipolar cell receptive and projective fields. Vice versa, the predicted bipolar cell projective field was obtained by deconvolving the measured ganglion cell receptive field with the measured bipolar cell receptive field.

Supplemental references

Asari, H. and Meister, M. (2012). Divergence of visual channels in the inner retina. Nat Neurosci, 15, 1581–1589.

Awatramani, G. B. and Slaughter, M. M. (2000). Origin of transient and sustained responses in ganglion cells of the retina. J Neurosci, 20, 7087–7095.

Baccus, S. A. and Meister, M. (2002). Fast and slow contrast adaptation in retinal circuitry. Neuron, 36, 909–919.

Baccus, S. A., Ölveczky, B. P., Manu, M., and Meister, M. (2008). A retinal circuit that computes object motion. J Neurosci, 28, 6807–6817.

Cook, P. B., Lukasiewicz, P. D., and McReynolds, J. S. (2000). $GABA_c$ receptors control adaptive changes in a glycinergic inhibitory pathway in salamander retina. J Neurosci, 20, 806–812.

DeVries, S. H. (2000). Bipolar cells use kainate and AMPA receptors to filter visual information into separate channels. Neuron, 28, 847–856.

Geffen, M. N., Broome, B. M., Laurent, G., and Meister, M. (2009). Neural encoding of rapidly fluctuating odors. Neuron, 61, 570–586.

Geffen, M. N., de Vries, S. E. J., and Meister, M. (2007). Retinal ganglion cells can rapidly change polarity from Off to On. PLoS Biol, 5, e65.

Masland, R. H. (2012). The neuronal organization of the retina. Neuron, 76, 266–280.

Meister, M., Pine, J., and Baylor, D. A. (1994). Multi-neuronal signals from the retina: acquisition and analysis. J Neurosci Methods, 51, 95–106.

Ölveczky, B. P., Baccus, S. A., and Meister, M. (2003). Segregation of object and background motion in the retina. Nature, 423, 401–408.

Pang, J.-J., Gao, F., and Wu, S. M. (2004). Stratum-by-stratum projection of light response attributes by retinal bipolar cells of *Ambystoma*. J Physiol, 558, 249–262.

Pouzat, C., Mazor, O., and Laurent, G. (2002). Using noise signature to optimize spike-sorting and to assess neuronal classification quality. J Neurosci Methods, 122, 43–57.

Segev, R., Goodhouse, J., Puchalla, J., and Berry, M. J. (2004). Recording spikes from a large fraction of the ganglion cells in a retinal patch. Nat Neurosci, 7, 1154–1161.

Segev, R., Puchalla, J., and Berry, M. J. (2006). Functional organization of ganglion cells in the salamander retina. J Neurophysiol, 95, 2277–2292.

Vallerga, S. and Usai, C. (1986). Relation between light responses and dendritic branching in the salamander ganglion cells. Exp Biol, 45, 81–90.

Vaney, D. I., Sivyer, B., and Taylor, W. R. (2012). Direction selectivity in the retina: symmetry and asymmetry in structure and function. Nat Rev Neurosci, 13, 194–208.

Veruki, M. L. and Hartveit, E. (2009). Meclofenamic acid blocks electrical synapses of retinal AII amacrine and on-cone bipolar cells. J Neurophysiol, 101, 2339–2347.

Wu, S. M., Gao, F., and Maple, B. R. (2000). Functional architecture of synapses in the inner retina: segregation of visual signals by stratification of bipolar cell axon terminals. J Neurosci, 20, 4462–4470.

Zhang, A.-J. and Wu, S. M. (2009). Receptive fields of retinal bipolar cells are mediated by heterogeneous synaptic circuitry. J Neurosci, 29, 789–797.

Zhang, A.-J. and Wu, S. M. (2010). Responses and receptive fields of amacrine cells and ganglion cells in the salamander retina. Vision Res, 50, 614–622.